symmetry

IMPACT FACTOR 2.2

CITESCORE 5.4

Article

Higher-Order Derivative Corrections to Axion Electrodynamics in 3D Topological Insulators

R. Martínez von Dossow, A. Martín-Ruiz and Luis F. Urrutia

MDPI

https://doi.org/10.3390/sym17040581

symmetry

MDPI

Article

Higher-Order Derivative Corrections to Axion Electrodynamics in 3D Topological Insulators

R. Martínez von Dossow, A. Martín-Ruiz * and Luis F. Urrutia

Instituto de Ciencias Nucleares, Universidad Nacional Autónoma de México, Ciudad de México 04510, Mexico; ricardo.martinez@correo.nucleares.unam.mx (R.M.v.D.); urrutia@nucleares.unam.mx (L.F.U.)
* Correspondence: alberto.martin@nucleares.unam.mx

Abstract: Three-dimensional topological insulators possess surface-conducting states in the bulk energy gap, which are topologically protected and can be well described as helical 2 + 1 Dirac fermions. The electromagnetic response is given by axion electrodynamics in the bulk, leading to a Maxwell–Chern–Simons theory at the boundary, which is the source of the Hall conductivity. In this paper, we extend the formulation of axion electrodynamics such that it captures higher-derivative corrections to the Hall conductivity. Using the underlying 2 + 1 quantum field theory at the boundary, we employ thermal field theory techniques to compute the vacuum polarization tensor at finite chemical potential in the zero-temperature limit. Applying the derivative expansion method, we obtain higher-order derivative corrections to the Chern–Simons term in 2 + 1 dimensions. To first order the corrections, we find that the Hall conductivity receives contributions proportional to ω^2 and $\mathbf{k}^2$ from the higher-derivative Chern–Simons term. Finally, we discuss the electrodynamic consequences of these terms on the topological Faraday and Kerr rotations of light, as well as on the image monopole effect.

Keywords: axion electrodynamics; topological insulators; Chern–Simons theory

check for updates

Academic Editor: Michel Planat

Received: 10 March 2025
Revised: 5 April 2025
Accepted: 8 April 2025
Published: 10 April 2025

Citation: Martínez von Dossow, R.; Martín-Ruiz, A.; Urrutia, L.F. Higher-Order Derivative Corrections to Axion Electrodynamics in 3D Topological Insulators. *Symmetry* **2025**, *17*, 581. https://doi.org/10.3390/sym17040581

Copyright: © 2025 by the authors. Licensee MDPI, Basel, Switzerland. This article is an open access article distributed under the terms and conditions of the Creative Commons Attribution (CC BY) license (https://creativecommons.org/licenses/by/4.0/).

1. Introduction

The electromagnetic response of (3 + 1)D time-reversal-invariant topological insulators is described by a topological field theory akin to axion electrodynamics. The surface term, which corresponds to a (2 + 1)D Chern–Simons term, describes the anomalous Hall effect on the surface, which is the physical origin behind the topological magnetoelectric effect, a hallmark response of TIs encapsulated in the transverse Hall conductivity $\sigma_{yx}(\omega, \mathbf{k})$. The half-quantized Hall effect holds true only when the Fermi level lies within the bandgap. However, in reality, the Fermi level lies outside the gap, so it is within the finite density of states, in which case the Hall effect would not be quantized anymore. Furthermore, realistic materials often exhibit deviations from idealized theoretical predictions due to various mechanisms, such as disorder and impurity scattering, and a systematic investigation of these is fundamental for a better understanding of the topological transport. This motivates us to investigate higher-order derivative corrections to the anomalous Hall effect that may arise due to spatial variations in the fields.

Traditionally in the study of fermionic topological phases, the dependence of σ_{yx} on frequency is taken into account at most, and the dependence on momentum is considered irrelevant or even detrimental. This idea is linked to the fact that the most common methods for calculating this conductivity, Kubo's linear response theory and Boltzmann's semi-classical approximation, are strictly defined for constant electric fields or at most

with harmonic time dependence. However, recently in the literature, some indications have appeared that the dependence of the Hall conductivity σ_{yx} on momentum plays a fundamental role in new phenomena of great theoretical and applied interest.

The first of these findings is related to the study of $2+1$ bosonic topological phases [1–4], particularly photonic ones. As shown in these references, the existence of these new topological phases inevitably requires non-locality (i.e., dependence on momentum and frequency) of the optical parameters of the material, particularly of σ_{yx}. In Ref. [1], a model is presented where the lowest-order correction in the momentum for this parameter, $\sigma_{yx} = \sigma_0 - \sigma_2(ka)^2$, allows for the existence of topological photonic phases with Chern number ± 2. This model was subsequently embedded in a phenomenological extension of $2+1$ Chern–Simons theory in Ref. [2]. Unlike the fermionic case, these bosonic phases have been studied little, with the additional difficulty that they have eluded experimental determination until now, unlike the former for which there has been substantial work carried out in the laboratory.

Another property of quantum Hall states where the dependence of σ_{yx} on momentum plays an important role is in the description of Hall viscosity. Hall viscosity, analogous to Hall conductivity, is another measurable property of these quantum states [5,6]. As originally defined, it is related to the system's response to metric perturbations that can be realized through lattice vibrations. However, in Refs. [7,8], it has been shown that for systems where Galilean invariance holds and that are constituted by particles with an equal charge-to-mass ratio, this property can be determined solely from the electromagnetic response of the system, taking into account higher-order contributions in the momentum of the Hall conductivity. This relationship between viscosity and electromagnetic properties of the system provides a convenient alternative for the measurement of this parameter. Additionally, it has been shown that Hall viscosity is related to the so-called Wen-Zee shift, a topological property of the quantum Hall state [9]. In Ref. [10], we find another phenomenological proposal including higher-order derivatives in the fields, designed as an additional correction to axion electrodynamics in order to describe the response of new metamaterials. These novel metamaterials exhibit optical properties analogous to those of topological insulators, including Kerr and Faraday rotations. Notably, the presence of external sources in these materials does not lead to the emergence of dyonic charges, thereby circumventing the Witten effect.

The aim of this work is to investigate a more general response theory of (3 + 1)D topological insulators that includes corrections to the Hall conductivity due to higher-order derivative modifications as well as those due to the chemical potential. This work focuses on determining the anomalous Hall conductivity localized at the edge of the TI and associated with the electromagnetic response derived from the $(2+1)$-dimensional electrodynamics present there. In this way, the sought-after corrections will appear naturally from the calculation of radiative corrections generated by integrating fermionic excitations at the edge. These are encapsulated in the corresponding $(2+1)$-dimensional vacuum polarization tensor (VPT), which provides higher-order derivative corrections as well as modifications through the introduction of the chemical potential at zero temperature. Recalling that the usual formulation of axion electrodynamics in the $(3+1)$-dimensional bulk correctly describes TIs, we are interested in also showing how modifications at the edge induce a consistent extension of axion ED in the bulk, in relation to the proposal of Ref. [10]. As expected, higher-order corrections in the momentum will depend on the metric and will not carry universal topological fermionic information. However, as we mentioned above, they will be of crucial importance for bosonic topological phases. The use of VPT calculations to incorporate additional material properties into its electromagnetic response is of a very general nature. Specifically, it has proven highly useful for determining corrections to

the anomalous Hall effect in the case of a two-node Weyl semimetal with band tilt and anisotropy [11–13].

For completeness, we review the derivation of the anomalous Hall conductivity in the presence of a chemical potential, but to the zeroth order in momentum, using the Kubo formula and the semi-classical Boltzmann approximation that includes topological modifications via the Berry phase. For the moment, both methods are unable to produce higher-order corrections in momentum, which, however, appears quite naturally in a derivative expansion of the VPT. We also investigate the impact of the corrections we have found for σ_{yx} on the Fresnel coefficients that appear at a TI–dielectric interface. In particular, we discuss the modifications induced in the Kerr and Faraday rotations of an impinging electromagnetic wave, as well as the modifications to the magnetoelectric effect that occurs when an electric charge is placed near the insulator.

This paper is organized as follows. In Section 2, we review the electromagnetic response of a topological insulator. Section 2.1 deals with a review of axion electrodynamics, which is the lowest-lying order of the electromagnetic response of TIs. In Section 2.2, we introduce the microscopic Hamiltonian for the surface states of 3D TIs and show the emergence of the half-quantized Hall effect by employing the Kubo formula and the semi-classical Boltzmann approach. Section 3 focus on an extension of axion electrodynamics in (3 + 1) dimensions, which consistently accommodates higher-order derivative corrections appearing at the boundary, through the modified Maxwell's equations resulting in the bulk. The basic idea is that the constant parameters encoding the magnetoelectricity of each TI in the usual case are now promoted to differential operators in the coordinates transverse to the interface, whose specific form will be determined by the radiative corrections at the interface. In Section 4, we calculate the VPT at the insulator boundary. In Section 4.1, we show how the microscopic Hamiltonian described in Section IIb is embedded in a (2 + 1)D Dirac theory. We note that both the dimensions of the electromagnetic coupling f and the corresponding gauge field $\mathcal{A}_\mu$ in (2 + 1)D differ from their respective counterparts e and A_μ in (3 + 1)D. However, the product $f\,\mathcal{A}_\mu$ has the same dimensions as $e\,A_\mu$, allowing us to write the resulting effective electromagnetic action in terms of the electromagnetic field A_μ in (3 + 1)D, but restricted to take values only at the interface. In this way, we can identify the resulting effective current from the (2 + 1)D calculation with the surface current K^μ localized at the interface obtained from the modified axionic action. The derivative corrections in the transverse coordinates to the interface are subsequently identified with the radiative corrections obtained from the (2 + 1)D theory. We then calculate the effective action by integrating out the fermions in (2 + 1)D using the derivative expansion method. The result for the VPT is presented in Sections 4.2 and 4.3 and contains second-order derivative corrections, which we interpret directly in terms of the surface current K^μ, obtaining the sought-after modifications for the anomalous Hall conductivity. The extension to include finite density effects in the VPT is carried in Section 4.4 by employing the Matsubara substitution. The final results for the corrections to the anomalous Hall conductivity are presented in Section 4.5. These results modify the boundary conditions at the interface of the TI, as well as the Fresnel relations for an incident electromagnetic wave. In Section 5, we discuss the effect of such modifications on Kerr and Faraday rotations, while in Section 6, we investigate the changes induced in the magnetoelectric effect when a charge is placed near the interface of a TI and the vacuum. A summary and discussion is presented in Section 7. For the benefit of the reader, we provide a brief summary of the derivative expansion method in Apendix B. The remaining four appendices include some technical calculations indicated in the text.

2. Electromagnetic Response of Topological Insulators

2.1. Axion Electrodynamics

The effective field theory governing the electromagnetic response of topological insulators, independently of the microscopic details, is defined by the following action (in SI units):

$$S = \int d^4x \left[-\frac{1}{4\mu_0} F_{\mu\nu} F^{\mu\nu} + \frac{1}{2} F_{\mu\nu} \mathcal{M}^{\mu\nu} - \frac{e^2}{8\pi h}\, \theta(x)\, F_{\mu\nu} \tilde{F}^{\mu\nu} - A_\mu J^\mu \right], \tag{1}$$

where $F_{\mu\nu} = \partial_\mu A_\nu - \partial_\nu A_\mu$ is the electromagnetic tensor, $\mathcal{M}^{\mu\nu}$ is the magnetization–polarization tensor, and $\tilde{F}^{\mu\nu} = \frac{1}{2}\epsilon^{\mu\nu\alpha\beta} F_{\alpha\beta}$ is the dual electromagnetic field tensor. The coordinate-dependent axion field $\theta(x)$ is assumed to be nondynamical. The nontrivial topological property, a half-quantized quantum Hall effect, manifests only at the interface between two insulating phases with different topological orders, in which case the axion field is discontinuous across the interface.

In general, the linear magnetoelectric response of a material is described by the magnetoelectric tensor $\theta_{ij} = \frac{\partial M_j}{\partial E_i}\big|_{\mathbf{B}=0} = \frac{\partial P_j}{\partial B_i}\big|_{\mathbf{E}=0}$, which is constrained by the symmetries of the material. In the case of the well-known antiferromagnetic Cr_2O_3, the magnetoelectric tensor is of the form $\theta_{ij} = \mathrm{diag}(\theta_\parallel, \theta_\parallel, \theta_\perp)$, and hence, the effective field theory is derivable from the Lagrangian $\mathcal{L} = \kappa\, \theta_{ij} E_i B_j$, which breaks Lorentz invariance and hence cannot be regarded as an axion-like theory. In the case of topological insulators, the relevant contribution to the magnetoelectric effect is orbital (i.e., electronic band), in which case the linear magnetoelectric coupling becomes $\theta_{ij} = \theta\, \delta_{ij}$, thus implying an effective field theory defined by Equation (1), which is a Lorentz-invariant axion field theory.

The time-reversal symmetry of 3D TIs indicates that $\theta = 0, \pi$ (mod 2π), and hence, the θ-term in action (1) has no effect on Maxwell equations in the bulk. When $\theta = 0$, we have a standard dielectric, while $\theta = \pi$ describes a topological insulator. It is worth mentioning that the theory is applicable only for a certain class of 3D insulators, such as TR symmetric TIs and axion insulators. In topological magnetic insulators, θ is proportional to their magnetic order parameter, and the fluctuation produces a dynamical axion field, which is not captured by our theory.

Variation in action (1) gives rise to the equations of motion,

$$\partial_\mu \mathcal{D}^{\mu\nu} = J^\nu - \frac{e^2}{2\pi h}\, (\partial_\mu \theta)\, \tilde{F}^{\mu\nu}, \tag{2}$$

together with the Bianchi identity $\partial_\mu \tilde{F}^{\mu\nu} = 0$ arising from the definition of the electromagnetic tensor in terms of the potentials. Here, $\mathcal{D}^{\mu\nu} = \frac{1}{\mu_0} F^{\mu\nu} - \mathcal{M}^{\mu\nu}$ is the electromagnetic displacement tensor.

We consider the simplest case of a planar interface Σ at $z = 0$ between one topological insulator located in the region $z < 0$ (region 1) and the other placed in the region $z > 0$ (region 2). Each material is characterized by its permittivity (ϵ_i), permeability (μ_i), and magnetoelectric susceptibility (θ_i), with $i = 1, 2$. This configuration is depicted in Figure 1, and the boundary effects at the planar interface are introduced by taking $\theta(z) = \theta_2\, H(z) + \theta_1\, H(-z)$, where $H(x)$ is the Heaviside function.

Inhomogeneity in the permittivity ϵ and the permeability μ are limited to a finite discontinuity across the surface Σ, analogously to the axion field $\theta(z)$. This choice produces $\partial_\mu \theta(z) = n_\mu\, (\theta_2 - \theta_1)\delta(z)$, with $n_\mu = (0, \hat{\mathbf{n}})$, where $\hat{\mathbf{n}}$ is the unit normal to the interface shown in Figure 1. Consequently, from Equation (2), one reads the effective four-current

$$J^\nu_{\mathrm{S}}(x) = \frac{e^2}{2\pi h}\, \delta(z)\, (\theta_1 - \theta_2)\, n_\mu \tilde{F}^{\mu\nu} \equiv \delta(z)\, K^\nu, \tag{3}$$

which defines the effective current K^ν that lives at the interface and depends only on the coordinates (x^0, x, y). Current conservation can be directly verified, i.e., $\partial_\nu K^\nu = 0$. In vector notation, result (3) yields the following surface charge and current densities:

$$K^0 = -\sigma_{yx}\, c\, \hat{\mathbf{n}} \cdot \mathbf{B}, \qquad \mathbf{K} = \sigma_{yx}\, \hat{\mathbf{n}} \times \mathbf{E}, \tag{4}$$

where

$$\sigma_{yx} = \nu \frac{e^2}{2h}, \qquad \nu = (\theta_2 - \theta_1)/\pi \in \mathbb{Z}, \tag{5}$$

is the half-quantized anomalous Hall conductivity at the TI surface. Since $\theta_{1,2} = 0, \pi$ (mod 2π), at the interface between two insulating phases with different topological orders, one has $\nu = \pm 1$. Later, we shall discuss the physical meaning of ν.

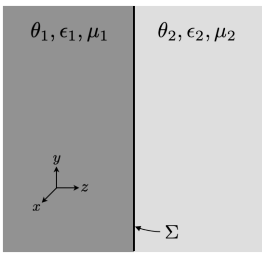

Figure 1. The left-half space is occupied by a topological insulator with dielectric constant ϵ_1, magnetic permeability μ_1, and magnetoelectric susceptibility θ_1. The right-half space is occupied by a topological insulator with dielectric constant ϵ_2, magnetic permeability μ_2, and magnetoelectric susceptibility θ_2.

The surface charge and current densities (4) are the origin of the topological magnetoelectric effect, which is a hallmark response of (3 + 1)D time-reversal-invariant topological insulators to external electric and magnetic fields. In order to better appreciate the emergence of the magnetoelectric response, it is convenient to express the equations of motion (2) in vector notation. The inhomogeneous Maxwell equations read

$$\nabla \cdot \mathbf{D} = \rho - \delta(z)\, \sigma_{yx}\, \hat{\mathbf{n}} \cdot \mathbf{B}, \qquad \nabla \times \mathbf{H} = \mathbf{J} + \delta(z)\, \sigma_{yx}\, \hat{\mathbf{n}} \times \mathbf{E}, \tag{6}$$

where $\mathbf{D} = \epsilon \mathbf{E}$ and $\mathbf{B} = \mu \mathbf{H}$ are the standard constitutive relations for a dielectric. The homogeneous Maxwell equations are untouched due to the gauge invariance of the theory. As evinced by Equation (6), Maxwell equations in the bulk contribute nothing from the axion coupling, such that all the dynamical modifications arise from the interface through the boundary conditions. There, the field-dependent current K^μ provides modifications to the Fresnel relations that connect the propagation modes from one media to the other. In assuming that the time derivatives of the fields are finite in the vicinity of surface Σ, field Equation (6) implies that the normal component of $\mathbf{D}$, as well as the tangential components of $\mathbf{H}$, acquire discontinuities that arise from the surface charge K^0 and current $\mathbf{K}$ densities, respectively. In the absence of external currents at the interface, the boundary conditions read

$$[\hat{\mathbf{n}} \cdot (\mathbf{D}_2 - \mathbf{D}_1)]_\Sigma = -\sigma_{yx}\, [\hat{\mathbf{n}} \cdot \mathbf{B}]_\Sigma, \qquad [\hat{\mathbf{n}} \times (\mathbf{H}_2 - \mathbf{H}_1)]_\Sigma = \sigma_{yx}\, [\hat{\mathbf{n}} \times \mathbf{E}]_\Sigma, \tag{7}$$

together with the continuity of the normal component of $\mathbf{B}$ and the tangential components of $\mathbf{E}$ at the interface, as usual. These boundary conditions encode the most salient feature of this theory: the topological magnetoelectric effect, where under an applied electric field, a quantized Hall current is induced on the surface, which in turn generates a magnetic

polarization, and vice versa. In other words, this is a 2 + 1-dimensional effect produced only when two insulating phases with different topological orders are assembled next to each other.

2.2. Surface Anomalous Hall Effect

Topological insulators are a nontrivial class of band insulators characterized by a topological invariant defined by the Bloch wave function in the Brillouin zone. As a manifestation of the nontrivial topology, TIs possess surface conducting states in the bulk energy gap that are topologically protected by time-reversal invariance and can be well described at low energies as helical Dirac fermions, which are robust against disorder. Once a TR-breaking perturbation is introduced on the surface, this helical state has a gap and is responsible for the topological magnetoelectric effect, as discussed above. The goal of this section is to review the low-energy model for the surface states to discuss the emergence of the anomalous Hall effect, which becomes half-quantized when the Fermi level lies in the gap and decays with the Fermi level when it crosses the gap. In addition, this model will be used in the next section to compute the higher-order corrections to the anomalous Hall effect.

The helical liquid on the gapped TI surface is described by a Dirac-like Hamiltonian

$$\hat{H}(\mathbf{k}) = \hbar v_F \mathbf{k} \cdot (\boldsymbol{\sigma} \times \hat{\mathbf{n}}) + m\sigma_z, \tag{8}$$

where $\boldsymbol{\sigma}$ is the vector formed out of Pauli matrices for the spin degree of freedom, $\mathbf{k}$ is the crystal momentum, and v_F is the Fermi velocity. The first term captures the gapless Dirac cone spectrum of the surface states, and the TR-breaking perturbation $m\sigma_z$ opens a gap at the Dirac point. Physically, the mass term can be induced by a ferromagnetic thin layer attached to the interface.

The eigenenergies of the Hamiltonian $\hat{H}(\mathbf{k})$ are calculated as

$$E_s(\mathbf{k}) = s\sqrt{(\hbar v_F k)^2 + m^2} \equiv s\lambda_k, \tag{9}$$

where $k = \sqrt{k_x^2 + k_y^2}$, and $s = \pm 1$ is the band index, and the corresponding surface eigenstates are

$$\Psi_{s\mathbf{k}}(\mathbf{r}) = \langle \mathbf{r} | \Psi_{s\mathbf{k}} \rangle = \frac{1}{\sqrt{2A}} \begin{pmatrix} s\sqrt{1 + s\Delta_k} \\ \sqrt{1 - s\Delta_k}\, e^{-i\theta_{\mathbf{k}}} \end{pmatrix} e^{i\mathbf{k}\cdot\mathbf{r}}, \tag{10}$$

where A is the area of the TI, $\Delta_k = m/\lambda_k$, and $\tan\theta_{\mathbf{k}} = k_x/k_y$. In Figure 2, we plot the dispersion of the energy bands for $v_F = 6 \times 10^5$ m/s and $m = 5$ meV. The dashed line corresponds to the gapless Dirac cone spectrum ($m = 0$). An important property of the system is the density of states (DOS), which is defined by $D(E) = \sum_{s,\mathbf{k}} \delta[E - E_s(\mathbf{k})]$. A simple calculation yields $D(E) = \frac{|E|}{2\pi\hbar^2 v_F^2} H(|E| - |m|)$. In Figure 2, we also plot the DOS in units of $D_0 = \frac{m}{2\pi\hbar^2 v_F^2}$ as a function of the energy. We observe that the DOS is zero for energies in the gap and jumps to a finite value exactly at $|E| = |m|$. The dashed red line corresponds to the case $m = 0$.

We now employ the Kubo formula to obtain the dc Hall conductivity, i.e.,

$$\sigma_{yx} = i\hbar \sum_{s \neq s'} \int_{\text{B.Z.}} \frac{d^2\mathbf{k}}{(2\pi)^2} \frac{d^2\mathbf{k}'}{(2\pi)^2} \{ f[E_s(\mathbf{k})] - f[E_{s'}(\mathbf{k}')] \} \frac{\langle \Psi_{s\mathbf{k}} | \hat{J}_x | \Psi_{s'\mathbf{k}'} \rangle \langle \Psi_{s'\mathbf{k}'} | \hat{J}_y | \Psi_{s\mathbf{k}} \rangle}{[E_s(\mathbf{k}) - E_{s'}(\mathbf{k}')]^2}, \tag{11}$$

where $f(E) = \left[1 + e^{\beta(E-E_F)}\right]^{-1}$ is the Fermi–Dirac distribution with $\beta = 1/k_B T$, where T is the temperature, and E_F is the Fermi level. The integral is taken over the Briollouin zone, and $\hat{\mathbf{J}} = (e/\hbar)\,\nabla_{\mathbf{k}}\,\hat{H}(\mathbf{k})$ is the current operator.

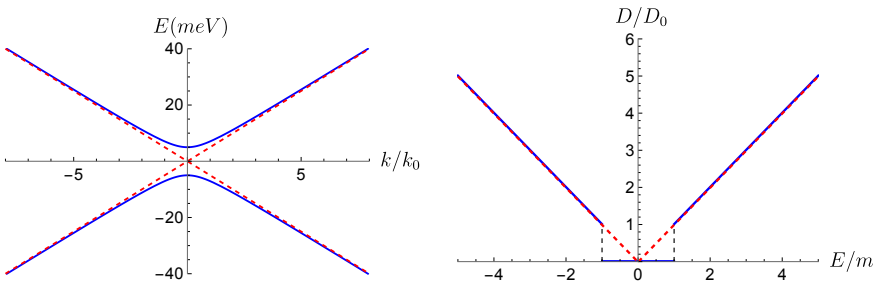

Figure 2. (**Left**): The continuous blue line corresponds to the energy dispersion as a function of the dimensionless parameter k/k_0, with $k_0 = m/\hbar v_F$, for $v_F = 6 \times 10^5$ m/s and $m = 5$ meV. The dashed curve corresponds to the gapless ($m = 0$) case. (**Right**): Density of states in units of $D_0 = \frac{m}{2\pi\hbar^2 v_F^2}$ as a function of E/m (continuous blue line). The dashed red line corresponds to the case $m = 0$.

In order to evaluate the conductivity, we need the matrix elements of the current operator. Using the Hamiltonian (8), we find $\hat{\mathbf{J}} = ev_F\,\boldsymbol{\sigma} \times \hat{\mathbf{n}}$, and hence, the required matrix elements become

$$\begin{aligned}
\langle \Psi_{s'\mathbf{k}'} | \hat{J}_x | \Psi_{s\mathbf{k}} \rangle &= i\frac{ev_F}{2}\left[s\sqrt{1+s\Delta_k}\sqrt{1-s'\Delta_k}e^{i\theta_{\mathbf{k}}} - s'\sqrt{1+s'\Delta_k}\sqrt{1-s\Delta_k}e^{-i\theta_{\mathbf{k}}}\right](2\pi)^2\delta(\mathbf{k}-\mathbf{k}'),\\
\langle \Psi_{s'\mathbf{k}'} | \hat{J}_y | \Psi_{s\mathbf{k}} \rangle &= -\frac{ev_F}{2}\left[s\sqrt{1+s\Delta_k}\sqrt{1-s'\Delta_k}e^{i\theta_{\mathbf{k}}} + s'\sqrt{1+s'\Delta_k}\sqrt{1-s\Delta_k}e^{-i\theta_{\mathbf{k}}}\right](2\pi)^2\delta(\mathbf{k}-\mathbf{k}').
\end{aligned} \tag{12}$$

Substituting Equation (12) into Equation (11), we obtain

$$\sigma_{yx} = -m\frac{\hbar e^2 v_F^2}{8\pi^2}\int_{\text{B.Z.}} \frac{d^2\mathbf{k}}{\lambda_k^3}\{f[E_+(\mathbf{k})] - f[E_-(\mathbf{k})]\}, \tag{13}$$

where we have used that

$$\sum_{s\neq s'}\{f[E_s(\mathbf{k})] - f[E_{s'}(\mathbf{k})]\}\frac{\langle \Psi_{s\mathbf{k}}|\hat{J}_x|\Psi_{s'\mathbf{k}'}\rangle\langle \Psi_{s'\mathbf{k}'}|\hat{J}_y|\Psi_{s\mathbf{k}}\rangle}{\left[E_s(\mathbf{k}) - E_{s'}(\mathbf{k}')\right]^2} = -im\frac{e^2 v_F^2}{2\lambda_k^3}\{f[E_+(\mathbf{k})] - f[E_-(\mathbf{k})]\}. \tag{14}$$

This gives the dc Hall conductivity at nonzero temperature. For zero temperature and with the Fermi level lying in the gap, the Fermi–Dirac distribution functions reduce to $f[E_+(\mathbf{k})] = 0$ and $f[E_-(\mathbf{k})] = 1$. Evaluating integral (13) in polar coordinates, we obtain

$$\sigma_{yx} = m\frac{\hbar e^2 v_F^2}{4\pi}\int_0^\infty \frac{kdk}{\lambda_k^3} = \frac{e^2}{2h}\frac{m}{|m|} = \text{sgn}(m)\,\frac{e^2}{2h}, \tag{15}$$

which is the half-quantized Hall conductivity at the TI surface. This result reveals that the factor $\nu = \pm 1$ appearing in the axion electrodynamics (4) is related to the direction of the magnetization of the magnetic impurities located at the interface to break TRS. When the Fermi level lies in the conduction band (i.e., $\mu > |m|$), the dc Hall conductivity at zero temperature is given by

$$\sigma_{yx} = -m\frac{\hbar e^2 v_F^2}{4\pi}\int_0^\infty \frac{kdk}{\lambda_k^3}[H(\mu - \lambda_k) - 1] = \frac{e^2}{2h}\frac{m}{\mu}. \tag{16}$$

Thus, when the Fermi level lies outside the gap, the Hall conductivity is not half-quantized anymore. In Figure 3, we plot the Hal conductivity as a function of the dimensionless chemical potential μ/m.

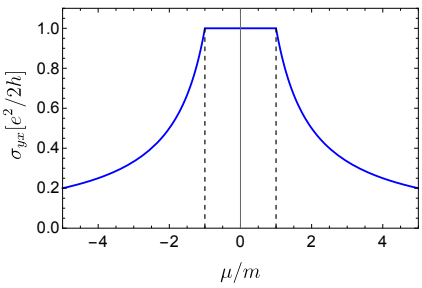

Figure 3. Hall conductivity (normalized by $e^2/2h$) as a function of the dimensionless parameter μ/m. It is half-quantized when the Fermi level lies in the bandgap and decreases inversely proportional to μ/m for filled bands.

Now, we shall evaluate the Hall conductivity using kinetic theory, which is a topologically modified semi-classical Boltzmann formalism used to describe the behavior of Dirac fermions. In the presence of an electric field, in addition to the usual band dispersion contribution, the velocity for Bloch electrons acquires an anomalous velocity proportional to the Berry curvature of the band, defined in terms of Bloch eigenstates by $\mathbf{\Omega}_s(\mathbf{k}) = i\langle\nabla_{\mathbf{k}}\Psi_{s\mathbf{k}}| \times |\nabla_{\mathbf{k}}\Psi_{s\mathbf{k}}\rangle$. Within kinetic theory, the contribution arising from the anomalous velocity defines the Hall conductivity as

$$\sigma_{ij} = \frac{e^2}{\hbar}\epsilon_{ijk}\sum_s \int_{\text{B.Z.}} \frac{d^2\mathbf{k}}{(2\pi)^2}[\mathbf{\Omega}_s(\mathbf{k})]_k f[E_s(\mathbf{k})]. \tag{17}$$

With the Bloch states (10), it is straightforward to obtain the Berry curvature:

$$\mathbf{\Omega}_s(\mathbf{k}) = s\frac{mv_F^2\hbar^2}{2\lambda_k^3}\,\hat{\mathbf{n}}, \tag{18}$$

And after further simplifications, the anomalous Hall conductivity can be written as

$$\sigma_{yx} = -m\frac{\hbar e^2 v_F^2}{8\pi^2}\int_{\text{B.Z.}} \frac{d^2\mathbf{k}}{\lambda_k^3}\sum_s s f[E_s(\mathbf{k})], \tag{19}$$

which is exactly Equation (13) derived using the Kubo formalism, and therefore, the resulting Hall conductivity is the same. The preceding methods are widely used by condensed matter theorists.

However, quantum field theory methods provide a third pathway to the anomalous Hall effect living on the interface between two TIs. The first step consists of embedding the theory of the helical liquid on a gapped TI surface (8) in an emergent Lorentz-invariant Dirac-like action in $2+1$ dimensions, which provides a good approximation only in a region close to the Dirac points in the Brillouin zone. Next, we identify the current density K^μ living on the surface, given by Equation (3), as the electromagnetic response of the relativistic fermionic excitations on the interface. This current can be obtained from the VPT $\Pi^{\mu\nu}$ in $2+1$ dimensions, through the relation $K^\mu = \Pi^{\mu\nu}A_\nu$. More importantly, quantum field theory methods provide a powerful route in cases where the Kubo formalism and kinetic theory cannot be applied. For example, they allow us to investigate the linear response to gradients of the electromagnetic fields, which is intimately related with the Hall viscosity in the case when the Galilean limit is taken in the emergent Dirac formulation [7,8]. Our main goal here is to investigate a more general electromagnetic response theory of (3 + 1)D topological insulators, which includes the response to gradients of the electromagnetic fields. To this end, we shall use a version of the derivative expansion method, which is well suited for computing the VPT $\Pi^{\mu\nu}$ as a series in the momenta k_0 and $\mathbf{k}$. Since the relevant

current is the transverse one, we focus on the respective contribution of the $\Pi^{\mu\nu}$, which is proportional to $\epsilon^{\mu\nu\rho}$ in $2+1$ dimensions.

3. Modified Axion Electrodynamics: Higher-Order Derivative Terms

Even though the calculation of the vacuum polarization effects in $2+1$ dimensions naturally introduces derivative corrections in the electromagnetic fields, we need to go one step backwards to make sure that this procedure constitutes a consistent extension of the standard axion electrodynamics in the bulk. We expect that the introduction of additional derivatives in the θ-term will inevitably destroy the topological features of the piecewise constant contributions previously described when $\theta = 0, \pi \pmod{2\pi}$. In this way, we propose a gauge-invariant modification to the θ-term in action (1), which is valid for arbitrary magnetoelectric materials, i.e., when their constant value of the magnetoelectrical polarizability is a real arbitrary number. In this case, θ's contribution to the action is odd under time reversal. In other words, we expect the higher-derivative terms to break time-reversal symmetry and be non-topological. We propose the following extension of the θ-term in action (1):

$$S_\theta = -\frac{e^2}{8\pi h}\int d^4x\; F_{\mu\nu}\hat{\mathcal{O}}_x\tilde{F}^{\mu\nu}, \tag{20}$$

where $\hat{\mathcal{O}}_x$ is a dimensionless operator to be determined. Nevertheless, notice that any constant contribution to $\hat{\mathcal{O}}_x$, which multiplies the Pontryagin density $F_{\mu\nu}\tilde{F}^{\mu\nu}$ and is integrated over a closed surface, will produce a topological contribution related to the first Chern number of the surface.

To begin with, we obtain some general properties of the operator $\hat{\mathcal{O}}_x$ and leave its detailed derivation for the next section. For an arbitrary two-dimensional interface at a given point, we choose $\hat{\mathcal{O}}_x$ as the product:

$$\hat{\mathcal{O}}_x = G(\xi)\,\hat{\mathcal{O}}_{\eta_\perp}(\partial_t, \partial_{\eta_1}, \partial_{\eta_2}), \tag{21}$$

where ξ is the coordinate parallel to the normal of the interface at that point, and η_1 and η_2 are the corresponding coordinates in the tangent space. The tensor structure of the Lagrangian density suggests that (20) and action $S_\theta = -\frac{e^2}{8\pi h}\int d^4x\; \tilde{F}_{\mu\nu}\hat{\mathcal{O}}_x F^{\mu\nu}$ must relate to the same equations of motion. This means that $\hat{\mathcal{O}}_x$ is an even function of the derivatives such that upon integrating by parts and disregarding boundary terms, one can transform the Lagrangian densities into each other. This means that in the lowest-order derivative extension, operator $\hat{\mathcal{O}}_x$ contains second-order derivatives in space and time. Finally, in the zeroth-order limit, one expects that $\hat{\mathcal{O}}_x$ reduces to the original position-dependent axion angle $\theta(x)$. The equations of motion for this model are obtained through variation in action (1), with the axion term replaced with the generalized contribution (20). One obtains

$$\partial_\mu \mathcal{D}^{\mu\nu} = J^\nu - \frac{e^2}{2\pi h}\left[\partial_\mu G(\xi)\right]\hat{\mathcal{O}}_{\eta_\perp}\,\tilde{F}^{\mu\nu}. \tag{22}$$

In addition, since we aim to describe higher-order derivative corrections to the anomalous effects on interface Σ, function $G(\xi)$ must be localized there, i.e., $\partial_\mu G(\xi) \sim n_\mu \delta(\Sigma)$, where n_μ is the normal to the surface at the given point.

For the configuration depicted in Figure 1, we write the coordinate dependence of operator $\hat{\mathcal{O}}_x$ as

$$\hat{\mathcal{O}}_x = H(z)\theta_2\;(1+\ell_2^2\hat{\mathcal{P}}_{2x_\perp}) + H(-z)\theta_1\;(1+\ell_1^2\hat{\mathcal{P}}_{1x_\perp}) \tag{23}$$

yielding

$$\partial_\mu \mathcal{D}^{\mu\nu} = J^\nu - \frac{e^2}{2\pi h}\,\delta(z)(\hat{\theta}_2 - \hat{\theta}_1)\,\tilde{F}^{\mu\nu}, \tag{24}$$

with operators

$$\hat{\theta}_i = \theta_i\,(1 + \ell_i^2 \hat{\mathcal{P}}_{ix_\perp}), \qquad a = 1, 2. \tag{25}$$

The constant contribution to these operators, due to the θ_i, reproduces the choice $\theta(z)$ in the piecewise axion angle of Section 2.1, which defines the topology of the phase. The notation $x^{\bar{\mu}}$ identifies the time plus the transverse coordinates $\mathbf{x}_\perp = (x, y)$, such that $x^{\bar{\mu}} = (x^0, x, y)$ (with $\bar{\mu} = 0, 1, 2$). The constant term reproduces the surface anomalous Hall conductivity σ_{yx}, and the second-order derivative operator $\hat{\mathcal{P}}_{x_\perp}$ encodes the higher-order derivative contributions at the interface, whose strength is driven by the length scales ℓ_i, which are determined using the microscopic parameters of the materials. For the configuration depicted in Figure 1, the surface current becomes

$$J_{\mathrm{S}}^\nu(x) = \frac{e^2}{2\pi h}\,\delta(z)\,n_\mu\,(\hat{\theta}_1 - \hat{\theta}_2)\,\tilde{F}^{\mu\nu} \equiv \delta(z)\,K^\nu, \tag{26}$$

where $n_\mu = (0, \hat{\mathbf{n}})$ is the unit normal to the interface. The corresponding surface charge and current densities are

$$K^0 = -\frac{e^2}{2\pi h}\,c\,\hat{\mathbf{n}} \cdot (\hat{\theta}_2 - \hat{\theta}_1)\mathbf{B}, \qquad \mathbf{K} = \frac{e^2}{2\pi h}\,\hat{\mathbf{n}} \times (\hat{\theta}_2 - \hat{\theta}_1)\mathbf{E}, \tag{27}$$

In referring to the current density $\mathbf{K}$, the unit operator in each $\hat{\theta}_i$ leads to the half-quantized anomalous Hall current $\nu \frac{e^2}{2h}\,\hat{\mathbf{n}} \times \mathbf{E}$. The second term includes higher-order derivatives of the electric field, $\ell_i^2\,\hat{\mathbf{n}} \times \hat{\mathcal{P}}_{ix_\perp}\mathbf{E}$. Regarding the momentum space in the case of a topological insulator at chemical potential μ, Fermi velocity v_F, and gap $m > \mu$, Equation (27) allows us to define the following frequency–momentum transverse conductivity:

$$\sigma_{yx}(\omega, \mathbf{k}_\perp, \mu) \;=\; \frac{e^2}{2\pi h}\Big(\tilde{\theta}_2 - \tilde{\theta}_1\Big), \tag{28}$$

where $\mathbf{k}_\perp = (k_x, k_y, 0)$, and quantities $\tilde{\theta}_a$ are the Fourier transforms of operators $\hat{\theta}_a$. In the static limit $\omega \to 0$ and $k_\perp \to 0$, $\sigma_{yx}(\omega, \mathbf{k}_\perp, \mu)$ approaches the universal half-quantized value $\mathrm{sgn}(m)\,\frac{e^2}{2h}$. However, in general, σ_{yx} has a nontrivial dependence on the wave number $k_\perp$ and the chemical potential μ. In addition, one expects the lengths scales ℓ_a to be a function of the material parameters, v_F, μ, and m.

For the completeness of this section and for later use, we write the modified field equations corresponding to the configuration depicted in Figure 1, including the higher-derivative corrections, as

$$\nabla \cdot \mathbf{D} = \rho - \delta(z)\,\frac{e^2}{2\pi h}\,\hat{\mathbf{n}} \cdot (\hat{\theta}_2 - \hat{\theta}_1)\mathbf{B}, \qquad \nabla \times \mathbf{H} = \mathbf{J} + \delta(z)\,\frac{e^2}{2\pi h}\,\hat{\mathbf{n}} \times (\hat{\theta}_2 - \hat{\theta}_1)\mathbf{E}, \tag{29}$$

which yield the following boundary conditions at the interface:

$$[\hat{\mathbf{n}} \cdot (\mathbf{D}_2 - \mathbf{D}_1)]_\Sigma = -\frac{e^2}{2\pi h}\,\hat{\mathbf{n}} \cdot [(\hat{\theta}_2 - \hat{\theta}_1)\mathbf{B}]_\Sigma, \qquad [\hat{\mathbf{n}} \times (\mathbf{H}_2 - \mathbf{H}_1)]_\Sigma = \frac{e^2}{2\pi h}\,\hat{\mathbf{n}} \times [(\hat{\theta}_2 - \hat{\theta}_1)\mathbf{E}]_\Sigma. \tag{30}$$

The analysis above shows us that one can consistently include higher-order derivative corrections to the anomalous Hall effect, which could be related to the Hall viscosity of the fermion fluid at some limit, through an appropriate extension of the $(3+1)$ axion electrodynamic contribution. The questions that remain open are the exact form of the

operators $\hat{\theta}_i$ and the definition of the length scales ℓ_i in terms of the material parameters. The next Section 4 is devoted to answering these question in detail using methods of relativistic thermal quantum field theory in $(2+1)$ dimensions.

4. The Vacuum Polarization Tensor in $(2+1)$ Dimensions

4.1. The Effective Field Theory at the Boundary

The primary objective of this section is to calculate the surface current K^μ induced by the helical liquid on the topological insulator surface, extending beyond the standard approximation that yields the anomalous Hall effect and leading to the sought-after corrections (29) to axion electrodynamics. This approach incorporates higher-order derivative corrections. To achieve this, we derive the corresponding VPT $\Pi^{\mu\nu}$ within the one-loop approximation of the $(2+1)$-dimensional effective action at the boundary. In other words, we consider K^μ as the electromagnetic response of the fermions living at the interface Σ (i.e., the surface states) and obtain its expression from the radiative corrections induced by their coupling to the electromagnetic field.

As a first step, we express the theory of the helical liquid on gapped TI surface (8) in a fully covariant way as a consequence of the emergent approximation that preserves Lorentz symmetry. To do this, we choose the following representation for the Dirac matrices:

$$\gamma_0 = \sigma_z, \qquad \gamma_1 = -i\sigma_x, \qquad \gamma_2 = -i\sigma_y, \tag{31}$$

where σ_i are the standard Pauli matrices. In this case, the theory of the helical liquid is described by a $(2+1)$ dimensional quantum field theory with the action

$$S = \int d^3\,\bar{x}\,\bar{\Psi}\Big[v_F\gamma^{\bar{\mu}}\left(i\hbar\partial_{\bar{\mu}} - f\mathcal{A}_{\bar{\mu}}\right) - mv_F^2\Big]\Psi, \tag{32}$$

where Ψ is a two-component Dirac spinor coupled to the electromagnetic gauge field $\mathcal{A}_{\bar{\mu}}$, and $\mathcal{F}_{\bar{\mu}\bar{\nu}} = \partial_{\bar{\mu}}\mathcal{A}_{\bar{\nu}} - \partial_{\bar{\nu}}\mathcal{A}_{\bar{\mu}}$ is the field strength. In addition, we introduce the coupling constant f and mass $m \equiv \Delta/v_F^2$, and we use the coordinates $x^{\bar{\mu}} = (v_F t, x, y)$, which we denote collectively as $\bar{x} = (v_F t, x_\perp)$. We can easily verify that the resulting Dirac Hamiltonian stemming from action (32) when $\mathcal{A}_{\bar{\mu}} = 0$ corresponds to Equation (8) for the gapped helical liquid.

Before proceeding with the technical details, it is essential to clarify the subtleties involved in embedding the (2 + 1)D effective field theory within the (3 + 1)D topologically insulating phase. A crucial point to emphasize is that the field $\mathcal{A}_\mu$ and the coupling constant f in the (2 + 1)D theory differ from the corresponding quantities in the (3 + 1)D case. This can be seen directly through a dimensional analysis, which for simplicity we perform in units of mass ($\hbar = v_F = 1$). We denote the dimension of the quantity inside the brackets by $[\,\cdot\,]$, and the factor m to some power on the right stands for the dimensionality of the object in units of mass. Therefore, we have $[f] = [\mathcal{A}_{\bar{\mu}}] = \mathrm{m}^{1/2}$ in $(2+1)$D, while in the $(3+1)$D case, e is dimensionless and $[A_\mu] = \mathrm{m}$. However, the relation

$$[f\mathcal{A}_{\bar{\mu}}] = [eA_{\bar{\mu}}] = \mathrm{m}. \tag{33}$$

between the dimensions of the product (field $\times$ coupling constant) is valid and will be crucial to correctly interpret how we connect the calculation of the surface curreny $K^{\bar{\mu}}$ in $(2+1)$ dimensions to axion electrodynamics in $(3+1)$ dimensions.

As we show in the next section, the fermionic coupling in (32) will generate the following contribution to the effective action:

$$S_{\text{eff}} = -\frac{f^2}{2\pi^2 h}\int d^3\bar{x}\,\frac{1}{2}\epsilon^{\bar{\mu}\bar{\nu}\bar{\rho}}\mathcal{A}_{\bar{\mu}}(\bar{x})(\hat{\theta}_2-\hat{\theta}_1)\,\partial_{\bar{\nu}}\mathcal{A}_{\bar{\rho}}(\bar{x}), \tag{34}$$

where $(\hat{\theta}_2 - \hat{\theta}_1)$ is the dimensionless operator introduced in the previous section. Here, $\epsilon^{\bar{\mu}\bar{\nu}\bar{\rho}}$ is the $(2+1)$D Levi-Civita tensor in the transverse space with $\epsilon^{012} = \epsilon^{0123} = 1$. The $(2+1)$D current $K^{\bar{\mu}}(\bar{x})$ is obtained as the functional derivative $\delta S_{\text{eff}}/\delta\mathcal{A}_{\bar{\mu}}(\bar{x})$ yielding

$$K^{\bar{\mu}}(\bar{x}) = -\frac{f^2}{4\pi^2 h}\,\epsilon^{\bar{\mu}\bar{\nu}\bar{\rho}}(\hat{\theta}_2-\hat{\theta}_1)\,\tilde{\mathcal{F}}_{\bar{\nu}\bar{\rho}}, \tag{35}$$

and has dimensiones $[K^{\bar{\mu}}(\bar{x})] = \text{m}^2$.

Let us recall that our aim is to obtain the modifications to axion electrodynamics in Equation (29), which arise exclusively from effective action (34) at the interface, thus avoiding phenomenological contributions. Then, it is crucial that we show how to consistently embed this result in the $(3+1)$D theory defined by action (20). To this end, we go back to the bulk, substitute operator (23) into action (20), and integrate by parts, obtaining

$$S_\theta = -\frac{e^2}{2\pi^2 h}\int d^4x\,\delta(z)\,\frac{1}{2}\epsilon^{\mu\nu\alpha\beta}n_\beta\,A_\mu(x)\,(\hat{\theta}_2-\hat{\theta}_1)\partial_\nu A_\alpha(x). \tag{36}$$

Next, we separate the electromagnetic potential in the form $(3+1) = (2+1)\oplus 1$ as $A_\mu(x) = A_{\bar{\mu}}(x_\perp) + n_\mu A_3(x)$, with $n_\mu = \delta_{\mu 3}$. Substituting A_μ into action (36), we obtain

$$S_\theta = -\frac{e^2}{2\pi^2 h}\int_\Sigma d^3\bar{x}\,\frac{1}{2}\epsilon^{\bar{\mu}\bar{\nu}\bar{\alpha}3}\,A_{\bar{\mu}}(\bar{x})\,(\hat{\theta}_2-\hat{\theta}_1)\partial_{\bar{\nu}}A_{\bar{\alpha}}(\bar{x}), \tag{37}$$

after integrating the z coordinate. The remaining integration $\int_\Sigma d^3\bar{x}$ implies that even though the integral is defined in terms of the $(3+1)$D electromagnetic potential A_μ, the integration domain is restricted to the interface. Relation (33) guarantees that we can identify the $(2+1)$-dimensional action (34) with the dimensionally reduced action (37), verifying that the response of the $(3+1)$D medium at the interface is indeed induced by the $(2+1)$D fermions living there.

In a similar manner and for later use, we follow the same idea to embed the $(2+1)$D VPT into the corresponding $(3+1)$D expression. We start with the general form of the effective action in $(2+1)$D, i.e.,

$$S_{\text{eff}} = \frac{1}{2}f^2\int d^3\bar{x}\,d^3\bar{x}'\,\mathcal{A}_{\bar{\mu}}(\bar{x})\,\Pi^{\bar{\mu}\bar{\nu}}(\bar{x}-\bar{x}')\,\mathcal{A}_{\bar{\nu}}(\bar{x}'), \tag{38}$$

where $\Pi^{\bar{\mu}\bar{\nu}}(\bar{x}-\bar{x}')$ is the $(2+1)$D VPT, with the units $[\Pi^{\bar{\mu}\bar{\nu}}] = \text{m}^4$. Again, we read the above relation as describing an action restricted to a $(2+1)$ surface embedded in $(3+1)$ dimensions, in terms of the four-dimensional vector potential A_μ and the physical coupling e:

$$S_{\text{eff}} = \frac{1}{2}e^2\int d^3\bar{x}\,d^3\bar{x}'\,A_{\bar{\mu}}(\bar{x})\,\Pi^{\bar{\mu}\bar{\nu}}(\bar{x}-\bar{x}')\,A_{\bar{\nu}}(\bar{x}'). \tag{39}$$

Nevertheless, when considering the momentum space, we must take only the three-dimensional Fourier transform since all the quantities in (39) depend only on the coordinates $x^{\bar{\mu}} = (x^0, x, y)$. Then, we obtain

$$S_{\text{add}} = e^2\frac{1}{2}\int d^3k\,A_{\bar{\mu}}(-k)\Pi^{\bar{\mu}\bar{\nu}}(k)A_{\bar{\nu}}(k), \tag{40}$$

with $[A_{\bar{\mu}}(k)] = 1/\mathrm{m}^2$ and $[\Pi^{\bar{\mu}\bar{\nu}}(k)] = \mathrm{m}$. The resulting current is

$$K^{\bar{\mu}}(k) = e^2\,\Pi^{\bar{\mu}\bar{\nu}}(k)A_{\bar{\nu}}(k), \tag{41}$$

with dimensions m^{-1}, as appropriate for the Fourier transform of $K^{\bar{\mu}}(x)$. A comparison with (26) in the momentum space yields

$$K^{\bar{\mu}}(k) = \frac{e^2}{2\pi h}\,n_{\bar{\nu}}\,(\hat{\theta}_1 - \hat{\theta}_2)\,\tilde{F}^{\bar{\nu}\bar{\mu}}(k) = -\frac{e^2}{2\pi h}(\tilde{\theta}_1 - \tilde{\theta}_2)\epsilon^{\bar{\mu}\alpha\beta 3}F_{\alpha\beta}(k) = e^2\Pi^{\bar{\mu}\bar{\nu}}(k)A_{\bar{\nu}}(k), \tag{42}$$

where $\tilde{\theta}_i$ denotes the sought-after momentum-dependent quantities input into Equation (29). Since the transverse contribution to $\Pi^{\bar{\mu}\bar{\nu}}(k)$, which is proportional to $\epsilon^{\bar{\mu}\bar{\nu}\bar{\rho}}$, has to be gauge-invariant, we can write

$$\Pi^{\bar{\mu}\bar{\nu}}(k) = i\epsilon^{\bar{\mu}\bar{\nu}\bar{\rho}}\Pi_T(k)k_{\bar{\rho}}, \qquad \epsilon^{012} = \epsilon^{0123} = +1, \tag{43}$$

such that the right-hand side of Equation (42) reads

$$\Pi^{\bar{\mu}\bar{\nu}}(k)A_{\bar{\nu}} = i\Pi_T(k)\,\epsilon^{\bar{\mu}\bar{\nu}\bar{\rho}}k_{\bar{\rho}}A_{\bar{\nu}} = \frac{1}{2}\,\Pi_T(k)\,\epsilon^{\bar{\mu}\bar{\nu}\bar{\rho}}F_{\bar{\nu}\bar{\rho}}, \tag{44}$$

Comparing Equations (42) and (44), we read

$$\frac{1}{\pi h}(\tilde{\theta}_2 - \tilde{\theta}_1) = \Pi_T(k), \tag{45}$$

yielding the final expression for sought-after derivative corrections to axion electrodynamics in (29), in terms of the effective action at the interface. In fact, they are fully contained in the exact expression of $\Pi_T(k)$. Nevertheless, in studying some applications, we will restrict ourselves to the lower-order result, which includes up to quadratic corrections in the momentum.

4.2. The Effective Action

We start with the Lagrangian density for quantum electrodynamics in $(2+1)$D, which we read from Equation (32). For simplicity in the notation, henceforth we do not write overlined indices (i.e., $\bar{\mu} \to \mu$) and we understand that all the quantities are in (2 + 1) dimensions. Therefore, the QED Lagrangian we consider is

$$\mathcal{L}_\Psi = \bar{\Psi}[v_F(i\hbar\not{\partial} + e\not{A}) - \Delta]\Psi, \tag{46}$$

where we use the slash notation $\not{Q} = \gamma^\mu Q_\mu$. Recall, our chosen representations for the Dirac matrices are $\gamma_0 = \sigma_z$, $\gamma_1 = -i\sigma_x$ and $\gamma_2 = -i\sigma_y$.

In the path integral formulation, the effective action $S_{\mathrm{eff}}[A]$ is defined as

$$e^{iS_{\mathrm{eff}}[A]/\hbar} = \int \mathcal{D}\bar{\psi}\,\mathcal{D}\psi\; e^{\frac{i}{\hbar}\int d^4x\,\mathcal{L}_\Psi} = \det[v_F(\hbar\not{p} + e\not{A}) - \Delta], \tag{47}$$

yielding

$$S_{\mathrm{eff}}[A] = -i\hbar\,\mathrm{Tr}\ln[v_F(\hbar\not{p} + e\not{A}) - \Delta], \tag{48}$$

with $i\partial_\mu = p_\mu$. In Appendix A, we provide a heuristic derivation of this result, which yields a series expansion of the effective action in powers of $\not{A}$. This is achieved by rewriting the operator as

$$v_F(\hbar\not{p} + e\not{A}) - \Delta = [v_F\hbar\not{p} - \Delta]\Big(1 + \frac{1}{[v_F\hbar\not{p} - \Delta]}\,v_F e\not{A}\Big), \tag{49}$$

taking the logarithm, and expanding $\ln(1-z) = -\sum_{n=1}^{\infty} \frac{1}{n} z^n$. Setting back the trace, we obtain

$$S_{\text{eff}}[A] = -i\hbar \,\text{Tr} \ln(\hbar v_F \not{p} - \Delta) + i\hbar \,\text{Tr} \sum_{n=1}^{\infty} \frac{(-1)^n}{n} \left[\frac{e}{\hbar} \frac{1}{\not{p} - m} \not{A} \right]^n, \tag{50}$$

where we define $m \equiv \Delta/(\hbar v_F)$. The first term on the right-hand side is an irrelevant constant independent of the potential. Since we are interested in the one-loop approximation (i.e., an action quadratic in A_μ), we consider only the term with $n = 2$. Therefore, the starting point of our calculation is

$$S_{\text{eff}}[A] = i\frac{e^2}{2\hbar} \,\text{Tr}[S(p)\not{A}S(p)\not{A}], \tag{51}$$

where $S(p) = (\not{p} - m)^{-1}$, and Tr includes the trace in coordinate space as well as in the Dirac matrix space. Note that $S(p)$ corresponds to the free fermionic propagator in natural units ($\hbar = v_F = 1$). Interestingly, the proportionality in Equation (51) depends only on the universal constants e and $\hbar$, while the material parameters as the energy gap Δ and the Fermi velocity v_F are included in the mass term.

Now, we come to the question of deriving the sought-after derivative corrections, which are simpler to deal with by having an expansion of the required quantities in powers of the momentum. In our case, this applies to the VPT derived from (51), which in general leads to a non-local function of the coordinates in the effective action. Thus, one way to obtain such power expansion is to look for a local expression of the effective action, in powers of the electromagnetic potential $A_\mu(x)$, from which we can directly read the expression for the VPT in powers of the momentum. This can be accomplished by calculating the trace of $S_{\text{eff}}^{(2)}$ in coordinate space using the version of the derivative expansion method briefly summarized in Appendix B. To this end, we start from the main identity of the derivative expansion method

$$A_\mu(x)S(p) = S(p - i\partial)A_\mu(x), \tag{52}$$

such that the effective action takes the form

$$S_{\text{eff}}[A] = i\frac{e^2}{2\hbar} \,\text{Tr}\left[S(p)\gamma^\mu S(p - i\partial)\gamma^\nu A_\mu(x)A_\nu(x)\right]. \tag{53}$$

Next, we compute the trace over the spatial coordinates, which is given by

$$S_{\text{eff}}[A] = i\frac{e^2}{2\hbar} \,\text{tr} \int d^3x \langle x| \left[S(p)\gamma^\mu S(p - i\partial)\gamma^\nu A_\mu(x)A_\nu(x)\right] |x\rangle, \tag{54}$$

where tr now indicates the trace over the Dirac matrices only. Inserting the completeness relation in momentum space, we obtain, in successive steps,

$$\begin{aligned} S_{\text{eff}}[A] &= i\frac{e^2}{2\hbar} \,\text{tr} \int d^3x \langle x| \left[S(p)\gamma^\mu S(p - i\partial) \int \frac{d^3p}{(2\pi)^3} |p\rangle \langle p| \gamma^\nu A_\mu(x)A_\nu(x) \right] |x\rangle, \\ &= i\frac{e^2}{2\hbar} \,\text{tr} \int d^3x \langle x|p\rangle \int \frac{d^3p}{(2\pi)^3} \left[S(p)\gamma^\mu S(p - i\partial)\gamma^\nu \langle p|x\rangle A_\mu(x)A_\nu(x)\right], \\ &= i\frac{e^2}{2\hbar} \,\text{tr} \int d^3x \int \frac{d^3p}{(2\pi)^3} \left[\frac{\not{p} + m}{p^2 - m^2} \gamma^\mu \frac{\not{p} - i\not{\partial} + m}{(p - i\partial)^2 - m^2} \gamma^\nu A_\mu(x)A_\nu(x) \right], \end{aligned} \tag{55}$$

where we use the product $\langle x|p\rangle\langle p|x\rangle = 1$. Then, we arrive at

$$S^{(2)}_{\text{eff}} = i\frac{e^2}{2\hbar}\int d^3x \int \frac{d^3p}{(2\pi)^3}\left\{\frac{\text{tr}\,\mathcal{N}^{\mu\nu}}{(p^2-m^2)[(p-i\partial)^2-m^2]}\right\}A_\mu(x)A_\nu(x), \tag{56}$$

with

$$\mathcal{N}^{\mu\nu} = (\gamma^\alpha p_\alpha + m)\gamma^\mu\left(\gamma^\beta p_\beta - i\gamma^\beta\partial_\beta + m\right)\gamma^\nu. \tag{57}$$

Let us emphasize that in expression (56), the derivative ∂ acts only on the potential $A_\mu(x)$. We observe that after expanding the denominator in (56), the resulting expression is indeed a local function of the electromagnetic potentials together with their derivatives.

Nevertheless, it is convenient to work in momentum space where

$$S^{(2)}_{\text{eff}} = i\frac{e^2}{2\hbar}\int \frac{d^3k}{(2\pi)^3}\int \frac{d^3p}{(2\pi)^3}\frac{\text{tr}\,\mathcal{N}^{\mu\nu}}{(p^2-m^2)[(p-k)^2-m^2]}\,A_\mu(k)A_\nu(-k), \tag{58}$$

and we identify k as the external momentum in the VPT. Now, we calculate the trace in matrix space. Some relevant properties for the chosen representation for the Dirac matrices are the following:

$$\text{tr}(\gamma^\mu) = 0, \quad \text{tr}(\gamma^\mu\gamma^\nu) = 2g^{\mu\nu}, \quad \text{tr}(\gamma^\mu\gamma^\nu\gamma^\rho) = -2i\epsilon^{\mu\nu\rho}, \quad \text{tr}(\gamma^\mu\gamma^\nu\gamma^\rho\gamma^\lambda) = 2(g^{\mu\nu}g^{\rho\lambda} - g^{\mu\rho}g^{\nu\lambda} + g^{\mu\lambda}g^{\nu\rho}), \tag{59}$$

where $g_{\mu\nu}$ is the Minkowski metric in $(2+1)$D. Using these relations, one obtains $\text{tr}\,\mathcal{N}^{\mu\nu} = \mathcal{N}^{\mu\nu}_0 + \mathcal{N}^{\mu\nu}_1(k) + \mathcal{N}^{\mu\nu}_{A1}(k)$ with

$$\mathcal{N}^{\mu\nu}_0 = 4p^\mu p^\nu - 2(p^2-m^2)g^{\mu\nu}, \qquad \mathcal{N}^{\mu\nu}_1(k) = -2p^\mu k^\nu + 2p_\alpha k^\alpha g^{\mu\nu} - 2p^\nu k^\mu, \qquad \mathcal{N}^{\mu\nu}_{A1}(k) = 2im\epsilon^{\mu\beta\nu}k_\beta. \tag{60}$$

The effective action can be written in terms of the VPT $\Pi^{\mu\nu}$ as

$$S^{(2)}_{\text{eff}} = \frac{e^2}{2}\int \frac{d^3k}{(2\pi)^3}A_\mu(k)\Pi^{\mu\nu}(k)A_\nu(-k), \tag{61}$$

where $\Pi^{\mu\nu}$ is given by

$$\Pi^{\mu\nu}(k) = i\frac{1}{\hbar}\int \frac{d^3p}{(2\pi)^3}\frac{\mathcal{N}^{\mu\nu}_0 + \mathcal{N}^{\mu\nu}_1(k) + \mathcal{N}^{\mu\nu}_{A1}(k)}{(p^2-m^2)[(p-k)^2-m^2]}. \tag{62}$$

Let us observe that we have factored out e^2 outside the integral in the effective action in such a way that our $\Pi^{\mu\nu}$ does not carry this factor. We observe the useful symmetry property

$$\Pi^{\mu\nu}(-k) = \Pi^{\nu\mu}(k), \tag{63}$$

following from Equation (61). As we mentioned previously, we are interested in finding derivative corrections to the contributions at the interface that are of topological origin in the zeroth-order approximation. In particular, we look for corrections to the anomalous Hall effect, which might be related to the Hall viscosity in a Galilean approximation of the relativistic calculation we pursue. What is relevant in this case is the transverse current that arises from the contribution proportional to $\epsilon^{\mu\nu\rho}$ in the VPT. The gauge invariance condition (43) together with the symmetry property (63) requires that the scalar $\Pi_T(K)$ be an even function of k_μ. This means that for our purposes, it is enough to retain only terms with odd powers in the external momentum when we expand the VPT. Also, the term proportional to $\epsilon^{\alpha\beta\gamma}$ in the VPT, which we call the "transverse" or "odd" part, is responsible for the boundary contributions in the axionic sector of the electromagnetic response of the media.

4.3. Expansion in Powers of the External Momentum

Now, we focus on the VPT defined by Equation (62) and expand the k-dependent denominator in powers of the external momenta. To this end, we use the series expansion $(A-B)^{-1} = A^{-1} + A^{-1}BA^{-1} + A^{-1}BA^{-1}BA^{-1} + \dots$ with the choice $A = (p^2 - m^2)$. The result is

$$\begin{aligned} \frac{1}{(p-k)^2 - m^2} &= \frac{1}{p^2 - m^2 - (2p_\lambda k^\lambda - k^2)}, \\ &= \frac{1}{p^2 - m^2}\left[1 + \frac{2p_\lambda k^\lambda - k^2}{p^2 - m^2} + \left(\frac{2p_\lambda k^\lambda - k^2}{p^2 - m^2}\right)^2 + \left(\frac{2p_\lambda k^\lambda - k^2}{p^2 - m^2}\right)^3 + \cdots\right]. \end{aligned} \tag{64}$$

Each term in the expansion depends on different powers of the external momenta. Since we are in the low-energy limit, this momentum is small compared with the mass m. Consequently, higher-order terms in k contribute increasingly smaller corrections, which justifies our expansion. For this reason, we consider only terms up to the third order in the momentum k, yielding the first higher-order derivative correction to the Chern–Simons term, which is the term of interest. Therefore, we decompose expansion (64) as follows:

$$[(p-k)^2 - m^2]^{-1} = \mathcal{D}_0 + \mathcal{D}_1(k) + \mathcal{D}_2(k) + \mathcal{D}_3(k) + \cdots, \tag{65}$$

where $\mathcal{D}_n(k)$ depends on the n-th power of the external momenta. From Equation (64), we read

$$\begin{aligned} &\mathcal{D}_0 = \frac{1}{p^2 - m^2}, \qquad \mathcal{D}_1(k) = \frac{2p_\lambda k^\lambda}{(p^2 - m^2)^2}, \qquad \mathcal{D}_2(k) = -\frac{1}{(p^2 - m^2)^2}k^2 + \frac{4p_\lambda p_\sigma}{(p^2 - m^2)^3}k^\lambda k^\sigma, \\ &\mathcal{D}_3(k) = -\frac{4p_\lambda}{(p^2 - m^2)^3}k^2 k^\lambda + \frac{8p_\lambda p_\sigma p_\eta}{(p^2 - m^2)^4}k^\lambda k^\sigma k^\eta. \end{aligned} \tag{66}$$

Therefore, the full expression for the VPT takes the form

$$\Pi^{\mu\nu}(k) = i\frac{1}{\hbar}\int \frac{d^3p}{(2\pi)^3}\,\frac{\mathcal{N}_0^{\mu\nu} + \mathcal{N}_1^{\mu\nu}(k) + \mathcal{N}_{A1}^{\mu\nu}(k)}{(p^2 - m^2)}\,[\mathcal{D}_0 + \mathcal{D}_1(k) + \mathcal{D}_2(k) + \mathcal{D}_3(k) + \cdots], \tag{67}$$

from where it is easy to identify specific terms by the number n of external momenta k.

In our approximation, the only relevant contributions to the VPT that are proportional to the Levi-Civita tensor containing one and three external momenta, are given by

$$\begin{aligned} \Pi_{\text{odd}}^{\mu\nu}(k) &= i\frac{1}{\hbar}\int \frac{d^3p}{(2\pi)^3}\,\frac{\mathcal{N}_{A1}^{\mu\nu}(k)}{(p^2 - m^2)}\,[\mathcal{D}_0 + \mathcal{D}_2(k)] \\ &= -\frac{2m}{\hbar}\epsilon^{\mu\beta\nu}k_\beta \int \frac{d^3p}{(2\pi)^3}\left[\frac{1}{p^2 - m^2} - \frac{1}{(p^2 - m^2)^3}k^2 + \frac{4p_\lambda p_\sigma}{(p^2 - m^2)^4}k^\lambda k^\sigma\right], \end{aligned} \tag{68}$$

which constitutes the starting point for the calculation of the VPT at finite density, after the truncation yields the sought-after first higher-order derivative correction to the Chern-Simons term.

Let us begin with the case of zero chemical potential, where the momentum integration is unbounded. Using the identity

$$\int_{-\infty}^{+\infty} \frac{d^3p}{(2\pi)^3}\, f(p^2)\, p^\mu p^\nu = \frac{g^{\mu\nu}}{3}\int_{-\infty}^{+\infty} \frac{d^3p}{(2\pi)^3}\, f(p^2)\, p^2, \tag{69}$$

yields

$$\Pi^{\mu\nu}_{\rm odd}(k) = -\frac{2m}{\hbar}\epsilon^{\mu\beta\nu}k_\beta \int \frac{d^3p}{(2\pi)^3}\left[\frac{1}{p^2-m^2} - \frac{1}{(p^2-m^2)^3}k^2 + \frac{4}{3}\frac{p^2}{(p^2-m^2)^4}k^2\right]$$
$$\equiv -\frac{2m}{\hbar}\epsilon^{\mu\beta\nu}k_\beta\left[I^0_2(m) - k^2\, I^0_3(m) + \frac{4}{3}k^2\, I^1_4(m)\right], \tag{70}$$

where we have introduced the mass-dependent integral

$$I^\beta_\alpha(m) = \int \frac{d^3p}{(2\pi)^3}\,\frac{(p^2)^\beta}{(p^2-m^2)^\alpha}, \tag{71}$$

which is calculated with full generality in Appendix C, as well as evaluated for the particular cases required in our approximation. Using the resulting values for the integral, we obtain

$$\Pi^{\mu\nu}_{\rm odd}(k) = -\frac{i}{4\pi\hbar}\,{\rm sgn}(m)\,\epsilon^{\mu\beta\nu}k_\beta\left(1+\frac{1}{12}\frac{k^2}{m^2}\right), \tag{72}$$

where ${\rm sgn}(m)$ is the sign function of m. The first contribution of (72) is the standard Chern–Simons term, while the second term is its first higher-order derivative correction. Notice that this contribution is no longer topological since it depends on the metric through $k^2 = k^\mu\eta_{\mu\nu}k^\nu$. Summarizing, the corrections for the transverse part of the vacuum polarization we obtain at this stage are

$$\Pi^{\mu\nu}_{\rm odd}(k) = i\epsilon^{\mu\nu\beta}k_\beta\,\pi_{\rm CS}, \qquad \pi_{\rm CS} = \frac{1}{2h}\,{\rm sgn}(m)\left(1+\frac{1}{12}\frac{k^2}{m^2}\right). \tag{73}$$

4.4. Vacuum Polarization Tensor at Finite Density

As pointed out, the previous result (73) is valid for a vanishing chemical potential, i.e., when the valence band is filled. However, in reality, the chemical potential lies outside the gap, so it is within the finite density of states. In the following, we incorporate the effects of a chemical potential μ because its location will determine the filling of the conduction and the valence bands. To this end, we use the Matsubara imaginary-time formalism to correctly incorporate the μ-dependence in the VPT. This technique is implemented through the substitution

$$\int \frac{d^3p}{(2\pi)^3}\,F(p_0,\mathbf{p}) \quad\to\quad +iT\sum_{n=-\infty}^{\infty}\int\frac{d^2\mathbf{p}}{(2\pi)^2}\,F(p_0,\mathbf{p}), \tag{74}$$

in our expression for the odd part of VPT (68). In Equation (74), $p_0 \to \tilde{p}_0 = (i\omega_n + \mu)$, the sum is over the Matsubara frequencies $\omega_n = (2n+1)\pi T$, and $F(p_0,\mathbf{p})$ is the integrand appearing in Equation (68). To obtain the contribution at finite chemical potential at zero temperature, we consider the following limit

$$\lim_{T\to 0} T\sum_{n=-\infty}^{\infty} F(p_0,\mathbf{p}) = \int\frac{dp_0}{2\pi i}\,F(p_0,\mathbf{p}) + \sum_{p_0^*<\mu}{\rm Res}[F(p_0,\mathbf{p}),p_0^*], \tag{75}$$

where p_0^* denotes the location of the poles in p_0 of $F(p_0,\mathbf{p})$, and "Res$[\,\cdot\,]$" refers to the corresponding residue. The first contribution corresponds to the usual term calculated in the previous subsection for $\mu = 0$, which is given by Equation (73) and termed $\Pi^{\mu\nu}_{\rm odd}(k)$. The second term corresponds to the zero temperature and finite chemical potential contribution [14,15], to be called $\tilde{\Pi}^{\mu\nu}_{\rm odd}(k,\mu)$. Clearly, these tensors should satisfy the limiting

condition $\tilde{\Pi}^{\mu\nu}_{\rm odd}(k,\mu=0)=\Pi^{\mu\nu}_{\rm odd}(k)$. In the following, we focus on the calculations of $\tilde{\Pi}^{\mu\nu}_{\rm odd}(k,\mu)$. We now introduce the functions

$$g^{(n)}(p_0,\mathbf{p})=\frac{1}{(p^2-m^2)^n},\qquad f^{(n)}_{\alpha\cdots\gamma}(p_0,\mathbf{p})=\frac{p_\alpha\cdots p_\gamma}{(p^2-m^2)^n},\tag{76}$$

such that the integrand in Equation (68) can be expressed in terms of these. Therefore, the chemical potential contribution to the VPT, at zero temperature, can be written as

$$\tilde{\Pi}^{\mu\nu}_{\rm odd}(k,\mu)=-2mi\hbar\epsilon^{\mu\beta\nu}k_\beta\int\frac{d^2\mathbf{p}}{(2\pi)^2}\sum_{p_0^*<\mu}\Big\{\mathrm{Res}[g^{(2)}(p_0,\mathbf{p}),p_0^*]-k^2\,\mathrm{Res}[g^{(3)}(p_0,\mathbf{p}),p_0^*]+4k^\lambda k^\sigma\,\mathrm{Res}[f^{(4)}_{\lambda\sigma}(p_0,\mathbf{p}),p_0^*]\Big\}.\tag{77}$$

The calculation of the residues is simple but not straightforward. We observe that functions $g^{(n)}(p_0,\mathbf{p})$ and $f^{(n)}_{\alpha\cdots\gamma}(p_0,\mathbf{p})$ have two simple poles of order n at $p^*_{0s}=s\sqrt{|\mathbf{p}|^2+m^2}$, with $s=\pm1$ labeling the poles, since the denominators can be rewritten in the form $(p^2-m^2)^n=(p_0-p^*_{0+})^n(p_0-p^*_{0-})^n$. Physically, the poles correspond to the conduction ($s=+1$) and valence ($s=-1$) bands, as suggested by the spectrum (9). Also, note that the position of the chemical potential determines the poles contributing to the summation in Equation (77). Here, we present the final results, and the technical details of the computation are relegated to Appendix D. The required residues in Equation (77) are

$$\mathrm{Res}[g^{(2)}(p_0,\mathbf{p}),p^*_{0s}]=-\frac{s}{4(|\mathbf{p}|^2+m^2)^{3/2}},\tag{78}$$

$$\mathrm{Res}[g^{(3)}(p_0,\mathbf{p}),p^*_{0s}]=\frac{3s}{16(|\mathbf{p}|^2+m^2)^{5/2}},\tag{79}$$

$$\mathrm{Res}[f^{(4)}_{\lambda\sigma}(p_0,\mathbf{p}),p^*_{0s}]=\frac{s\delta^0_\lambda\delta^0_\sigma}{32(|\mathbf{p}|^2+m^2)^{5/2}}-\frac{5sp_ip_j\delta^i_\lambda\delta^j_\sigma}{32(|\mathbf{p}|^2+m^2)^{7/2}}.\tag{80}$$

In substituting the residues in Equation (77), the chemical potential contribution to the VPT becomes

$$\tilde{\Pi}^{\mu\nu}_{\rm odd}(k,\mu)=\frac{2m}{i\hbar}\epsilon^{\mu\beta\nu}k_\beta\sum_{s=\pm1}s\int\frac{d^2\mathbf{p}}{(2\pi)^2}\left\{-\frac{1}{4(|\mathbf{p}|^2+m^2)^{3/2}}-\frac{3k^2-2k_0^2}{16(|\mathbf{p}|^2+m^2)^{5/2}}-\frac{5(\mathbf{p}\cdot\mathbf{k})^2}{8(|\mathbf{p}|^2+m^2)^{7/2}}\right\}H(\mu-p^*_{0s}),\tag{81}$$

where the Heaviside function implements the restriction of summing over the poles below the Fermi level. This double integral becomes easier to perform in polar coordinates, where the area element is $d^2\mathbf{p}=|\mathbf{p}|d|\mathbf{p}|d\phi$ with $\phi\in[0,2\pi)$, and where we choose the p_x axis in the direction of the vector $\mathbf{k}$. Noting that $\mathbf{p}\cdot\mathbf{k}=|\mathbf{p}||\mathbf{k}|\cos\phi$, the angular integration in Equation (81) yields

$$\tilde{\Pi}^{\mu\nu}_{\rm odd}(k,\mu)=i\frac{m}{2h}\epsilon^{\mu\beta\nu}k_\beta\sum_{s=\pm1}s\int_0^\infty|\mathbf{p}|d|\mathbf{p}|\left\{\frac{1}{(|\mathbf{p}|^2+m^2)^{3/2}}+\frac{3k^2-2k_0^2}{4(|\mathbf{p}|^2+m^2)^{5/2}}+\frac{5|\mathbf{p}|^2|\mathbf{k}|^2}{4(|\mathbf{p}|^2+m^2)^{7/2}}\right\}H(\mu-p^*_{0s}).\tag{82}$$

To evaluate this integral, we change the variable $|\mathbf{p}|$ to $p_0^*=\sqrt{|\mathbf{p}|^2+m^2}=p^*_{0s}/s$, such that $|\mathbf{p}|d|\mathbf{p}|=p_0^*dp_0^*$. Therefore,

$$\begin{aligned}\tilde{\Pi}^{\mu\nu}_{\rm odd}(k,\mu)&=i\frac{m}{8h}\epsilon^{\mu\beta\nu}k_\beta\sum_{s=\pm1}s\int_{|m|}^\infty\frac{dp_0^*}{p_0^{*2}}\left\{4+\frac{k^2+3|\mathbf{k}|^2}{p_0^{*2}}-\frac{5m^2|\mathbf{k}|^2}{p_0^{*4}}\right\}H(\mu-sp_0^*)\\&\equiv i\frac{m}{8h}\epsilon^{\mu\beta\nu}k_\beta\Big[4J_2(\mu,m)+(k^2+3|\mathbf{k}|^2)J_4(\mu,m)-5m^2|\mathbf{k}|^2J_6(\mu,m)\Big],\end{aligned}\tag{83}$$

where we introduce the integral

$$J_n(\mu, m) = \sum_{s=\pm 1} s \int_{|m|}^{\infty} \frac{dp_0^*}{p_0^{*n}} H(\mu - s p_0^*), \tag{84}$$

which we evaluate in detail in Appendix E. The calculation of this integral is simple but not straightforward, and the subtlety relies on the fact that there are two mass scales, $|m|$ and μ, such that the result of the integral depends on how these compare. With the result of Equation (A49) for the function $J_n(\mu, m)$ in the bandgap, i.e., for $\mu < |m|$, the VPT in Equation (83) is

$$\tilde{\Pi}^{\mu\nu}_{\text{odd}}(k, \mu) = -i \frac{1}{2h} \operatorname{sgn}(m)\, \epsilon^{\mu\beta\nu} k_\beta \left(1 + \frac{k^2}{12m^2}\right) H(|m| - \mu). \tag{85}$$

Equation (85) shows that the VPT in the bandgap is exactly the same as that for $\mu = 0$, given by Equation (73), thus implying that it is not affected by the position of the chemical potential as long as it lies inside the bandgap. Next, using the result of Equations (A48) and (A49), one can write the VPT in the region of finite density of states (i.e., for $|\mu| > |m|$) as

$$\tilde{\Pi}^{\mu\nu}_{\text{odd}}(k, \mu) = -i \frac{1}{2h} \frac{m}{|\mu|} \epsilon^{\mu\beta\nu} k_\beta \left[1 + \frac{k^2}{12\mu^2} + \frac{|\mathbf{k}|^2}{4\mu^2}\left(1 - \frac{m^2}{\mu^2}\right)\right] H(|\mu| - |m|), \tag{86}$$

with the Fermi level lying either in the valence band or in the conduction band.

4.5. Electromagnetic Response

From the VPT, (85), and (86), one can calculate the transverse current density from the expression

$$K^{\mu}_{\text{odd}}(\omega, \mathbf{k}) = e^2\, \tilde{\Pi}^{\mu\nu}_{\text{odd}}(\omega, \mathbf{k})\, A_\nu(\omega, \mathbf{k}). \tag{87}$$

On the other hand, recalling that $k_\beta = i\partial_\beta$, we can write $-i\epsilon^{\mu\beta\nu 3} k_\beta A_\nu = \tilde{F}^{\mu 3}$, where $\tilde{F}^{\mu\nu}$ is the dual electromagnetic field tensor in $(3+1)$D. Therefore, using Equation (85), the current density can be written as

$$K^{\mu}_{\text{odd}}(\omega, \mathbf{k}) = \frac{e^2}{2h} \operatorname{sgn}(m) \left(1 + \frac{k^2}{12m^2}\right) H(|m| - \mu)\, \tilde{F}^{\mu 3}, \tag{88}$$

in the bandgap, whilst in the finite density of states region, it becomes

$$K^{\mu}_{\text{odd}}(\omega, \mathbf{k}) = \frac{e^2}{2h} \frac{m}{|\mu|} \left[1 + \frac{k^2}{12\mu^2} + \frac{|\mathbf{k}|^2}{4\mu^2}\left(1 - \frac{m^2}{\mu^2}\right)\right] H(|\mu| - |m|)\, \tilde{F}^{\mu 3}. \tag{89}$$

Now, using the fact that $\tilde{F}^{23} = E^1 = E_x$ and defining the conductivity tensor by $K_{\text{odd}\, y} = \sigma_{yx} E_x$, we find

$$\sigma_{yx}(\omega, \mathbf{k}) = \frac{e^2}{2h} \operatorname{sgn}(m) \left(1 + \frac{k^2}{12m^2}\right) \tag{90}$$

for the chemical potential lying in the bandgap, and

$$\sigma_{yx}(\omega, \mathbf{k}) = \frac{e^2}{2h} \frac{m}{|\mu|} \left[1 + \frac{k^2}{12\mu^2} + \frac{|\mathbf{k}|^2}{4\mu^2}\left(1 - \frac{m^2}{\mu^2}\right)\right], \tag{91}$$

for $|\mu| > |m|$. Note also that the conductivity tensor is antisymmetric: $\sigma_{yx}(\omega, \mathbf{k}) = -\sigma_{xy}(\omega, \mathbf{k})$. As a consistency check, in the low-energy $\omega \to 0$ and long-wavelength $\mathbf{k} \to \mathbf{0}$ regimes, we have

$$\sigma_{yx}(0, \mathbf{0}) = \frac{e^2}{2h} \operatorname{sgn}(m)\, H(|m| - \mu), \qquad \sigma_{yx}(0, \mathbf{0}) = \frac{e^2}{2h} \frac{m}{|\mu|} H(|\mu| - |m|), \tag{92}$$

which is consistent with the result obtained in Section 2.2 with the use of the Kubo formula and the kinetic theory. This result reproduces the half-quantized Hall conductivity within the gap. General results (90) and (91) allow us to analyze other quantum Hall regimes. For example, at high frequencies ($\omega \sim$ THz) but low momentum, $\mathbf{k} \approx \mathbf{0}$, which is a regime well explored experimentally [16], Equations (90) and (91) predict

$$\sigma_{yx}(\omega, \mathbf{0}) = \frac{e^2}{2h} \operatorname{sgn}(m) \left(1 + \frac{\omega^2}{12m^2}\right) H(|m| - \mu), \qquad \sigma_{yx}(\omega, \mathbf{0}) = \frac{e^2}{2h} \frac{m}{|\mu|} \left(1 + \frac{\omega^2}{12\mu^2}\right) H(|\mu| - |m|). \tag{93}$$

5. Corrections to the Topological Kerr and Faraday Rotations

From Equation (30), we learn that the modified Hall conductivity $\sigma_{yx}(\omega, \mathbf{k}_\perp, \mu)$ in Equation (28) determines the boundary conditions at the interface of two topological insulators. We now investigate the impact of the higher-order derivative corrections to the Hall conductivity on the reflection matrices for a topological insulator–dielectric interface. We choose our coordinates such that the interface is defined by the plane $z = 0$. Let us assume that a plane wave with wave vector $\mathbf{k}_i$ impinges upon the interface from $z < 0$ (dielectric) towards the topological insulator occupying the region $z > 0$. The semi-infinite region $z < 0$ ($z > 0$) is characterized by the permittivity ϵ_1 (ϵ_2), the permeability μ_1 (μ_2), and the magnetoelectric susceptibility $\theta_1 = 0$ ($\theta_2 = \tilde{\theta}(k)$). The interface supports a surface Hall conductivity $\sigma_{yx}(\omega, \mathbf{k}_\perp, \mu)$ including derivative corrections. Let us select the plane of incidence to be the one determined by $\mathbf{k}_i$ and $\hat{\mathbf{e}}_z$. Owing to the rotational symmetry about z, without loss of generality, we can take our coordinate system so that this plane coincides with the xz plane, such that $\mathbf{k}_i = k_x \hat{\mathbf{e}}_x + k_z \hat{\mathbf{e}}_z$, as shown in Figure 4. The incident electromagnetic fields are then [17,18]

$$\mathbf{E}_i = \left[E_i^{\mathrm{TE}} \hat{\mathbf{e}}_y + E_i^{\mathrm{TM}} \frac{v_1}{\omega} (k_z \hat{\mathbf{e}}_x - k_x \hat{\mathbf{e}}_z)\right] e^{i(k_x x + k_z z - \omega t)}, \tag{94}$$

$$\mathbf{B}_i = \left[\frac{1}{v_1} E_i^{\mathrm{TM}} \hat{\mathbf{e}}_y - E_i^{\mathrm{TE}} \frac{1}{\omega} (k_z \hat{\mathbf{e}}_x - k_x \hat{\mathbf{e}}_z)\right] e^{i(k_x x + k_z z - \omega t)}, \tag{95}$$

where $k_z = \sqrt{(\omega/v_1)^2 - k_x^2}$, $v_1 = 1/\sqrt{\epsilon_1 \mu_1}$ is the speed of light in medium 1, and E_i^{TE} and E_i^{TM} are the field amplitudes for TE and TM polarizations, respectively. For the reflected wave, the momentum reads $\mathbf{k}_r = k_x \hat{\mathbf{e}}_x - k_z \hat{\mathbf{e}}_z$ and the electromagnetic fields become

$$\mathbf{E}_r = \left[E_r^{\mathrm{TE}} \hat{\mathbf{e}}_y - E_r^{\mathrm{TM}} \frac{v_1}{\omega} (k_z \hat{\mathbf{e}}_x + k_x \hat{\mathbf{e}}_z)\right] e^{i(k_x x - k_z z - \omega t)}, \tag{96}$$

$$\mathbf{B}_r = \left[\frac{1}{v_1} E_r^{\mathrm{TM}} \hat{\mathbf{e}}_y + E_r^{\mathrm{TE}} \frac{1}{\omega} (k_z \hat{\mathbf{e}}_x + k_x \hat{\mathbf{e}}_z)\right] e^{i(k_x x - k_z z - \omega t)}, \tag{97}$$

where E_r^{TE} and E_r^{TM} are the field amplitudes for TE and TM polarization, respectively. The transmitted wave is given by the fields inside the TI:

$$\mathbf{E}_t = \left[E_t^{\mathrm{TE}} \hat{\mathbf{e}}_y + E_t^{\mathrm{TM}} \frac{v_2}{\omega} (q_z \hat{\mathbf{e}}_x - k_x \hat{\mathbf{e}}_z)\right] e^{i(k_x x + q_z z - \omega t)}, \tag{98}$$

$$\mathbf{B}_t = \left[\frac{1}{v_2} E_t^{\mathrm{TM}} \hat{\mathbf{e}}_y - E_t^{\mathrm{TE}} \frac{1}{\omega} (q_z \hat{\mathbf{e}}_x - k_x \hat{\mathbf{e}}_z)\right] e^{i(k_x x + q_z z - \omega t)}, \tag{99}$$

where $q_z = \sqrt{(\omega/v_2)^2 - k_x^2}$, $v_2 = 1/\sqrt{\epsilon_2\mu_2}$ is the speed of light in medium 2, and $E_t^{\rm TE}$ and $E_t^{\rm TM}$ are the transmitted field amplitudes for TE and TM polarizations, respectively. Now we shall impose the boundary conditions (30), which for a topological insulator–dielectric interface read

$$[\epsilon\,\mathbf{E}\cdot\hat{\mathbf{n}}]_\Sigma = \hat{\mathbf{n}}\cdot\hat{\mathcal{O}}_{t,x}\,\mathbf{B}|_\Sigma, \qquad [\mathbf{B}\cdot\hat{\mathbf{n}}]_\Sigma = 0, \qquad [\mathbf{E}\times\hat{\mathbf{n}}]_\Sigma = \mathbf{0}, \qquad [(\mathbf{B}/\mu)\times\hat{\mathbf{n}}]_\Sigma = \hat{\mathbf{n}}\times\hat{\mathcal{O}}_{t,x}\,\mathbf{E}|_\Sigma, \tag{100}$$

where

$$\hat{\mathcal{O}}_{t,x} = \alpha\,\mathrm{sgn}(\Delta)\left[1 - \frac{\hbar^2 v_F^2}{12\Delta^2}(\partial_0^2 - \partial_x^2)\right] \tag{101}$$

and the chemical potential lies in the bandgap of the TI.

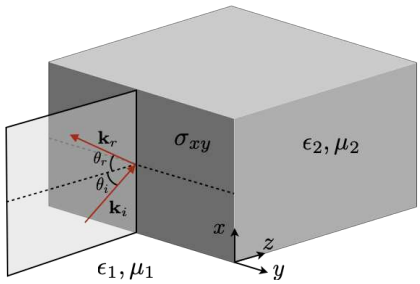

Figure 4. An incident plane wave impinging on a topological insulator. The interface supports a surface Hall effect with viscous corrections.

Note that for a plane wave, we have $\hat{\mathcal{O}}_{t,x}\mathbf{E} = \alpha\,\mathrm{sgn}(\Delta)\left[1 + \frac{\hbar^2 v_F^2}{12\Delta^2}(k_0^2 - k_x^2)\right]\mathbf{E} \equiv \tilde{\theta}(\omega, k_x)\,\mathbf{E}$, with $k_0 = \omega/v_F$.

Imposing the boundary conditions at $z = 0$, we obtain

$$\begin{aligned} E_t^{\rm TE} - E_i^{\rm TE} - E_r^{\rm TE} &= 0, \\ v_2 q_z E_t^{\rm TM} - v_1 k_z E_i^{\rm TM} + v_1 k_z E_r^{\rm TM} &= 0, \\ \frac{q_z}{\mu_2} E_t^{\rm TE} - \frac{k_z}{\mu_1}\left(E_i^{\rm TE} - E_r^{\rm TE}\right) &= +\tilde{\theta}(\omega, k_x) v_2\, E_t^{\rm TM} q_z, \\ \epsilon_2 v_2 E_t^{\rm TM} - \epsilon_1 v_1\left(E_i^{\rm TM} + E_r^{\rm TM}\right) &= -\tilde{\theta}(\omega, k_x)\, E_t^{\rm TE}. \end{aligned} \tag{102}$$

The solution to this system is quite simple. Defining the reflection matrix as

$$\begin{pmatrix} E_r^{\rm TE} \\ E_r^{\rm TM} \end{pmatrix} = \begin{pmatrix} R_{ss} & R_{sp} \\ R_{ps} & R_{pp} \end{pmatrix}\begin{pmatrix} E_i^{\rm TE} \\ E_i^{\rm TM} \end{pmatrix} \equiv \mathbf{R}(\omega, k_x)\begin{pmatrix} E_i^{\rm TE} \\ E_i^{\rm TM} \end{pmatrix}, \tag{103}$$

we find

$$\mathbf{R}(\omega, k_x) = \frac{1}{\gamma}\begin{pmatrix} (\epsilon_2 k_z + \epsilon_1 q_z)(\mu_2 k_z - \mu_1 q_z) - \mu_1\mu_2 k_z q_z \tilde{\theta}^2 & 2\mu_1\mu_2\epsilon_1 v_1 k_z q_z \tilde{\theta} \\ 2\mu_1\mu_2\epsilon_1 v_1 k_z q_z \tilde{\theta} & (\epsilon_2 k_z - \epsilon_1 q_z)(\mu_2 k_z + \mu_1 q_z) + \mu_1\mu_2 k_z q_z \tilde{\theta}^2 \end{pmatrix}, \tag{104}$$

and $\gamma = (\epsilon_1 q_z + \epsilon_2 k_z)(\mu_1 q_z + \mu_2 k_z) + \mu_1\mu_2 k_z q_z \tilde{\theta}^2$. Following the same procedure, one can further calculate the transmission matrix, defined by

$$\begin{pmatrix} E_t^{\rm TE} \\ E_t^{\rm TM} \end{pmatrix} \equiv \mathbf{T}(\omega, k_x)\begin{pmatrix} E_i^{\rm TE} \\ E_i^{\rm TM} \end{pmatrix}, \tag{105}$$

which becomes

$$\mathbf{T}(\omega, k_x) = \frac{1}{v_2\gamma}\begin{pmatrix} 2\mu_2 v_2 k_z(\epsilon_2 k_z + \epsilon_1 q_z) & 2\epsilon_1\mu_1\mu_2 v_1 v_2 k_z q_z \tilde{\theta} \\ -2k_z^2\mu_2\tilde{\theta} & 2k_z\epsilon_1 v_1(\mu_1 q_z + \mu_2 k_z) \end{pmatrix}. \tag{106}$$

At normal incidence ($k_x = 0$), we have $k_z = \omega/v_1$ and $q_z = \omega/v_2$. Therefore, the reflection matrix (104) becomes

$$\mathbf{R}(\omega, k_x = 0) = \frac{1}{\delta}\begin{pmatrix} (\epsilon_2 v_2 + \epsilon_1 v_1)(\mu_2 v_2 - \mu_1 v_1) - \sqrt{\frac{\mu_1}{\epsilon_1}\frac{\mu_2}{\epsilon_2}}\tilde{\theta}^2 & 2v_1 v_2 \mu_1\mu_2\epsilon_1 v_1\tilde{\theta} \\ 2v_1 v_2\mu_1\mu_2\epsilon_1 v_1\tilde{\theta} & (\epsilon_2 v_2 - \epsilon_1 v_1)(\mu_2 v_2 + \mu_1 v_1) + \sqrt{\frac{\mu_1}{\epsilon_1}\frac{\mu_2}{\epsilon_2}}\tilde{\theta}^2 \end{pmatrix}, \tag{107}$$

with $\delta = (\epsilon_2 v_2 + \epsilon_1 v_1)(\mu_2 v_2 + \mu_1 v_1) + \sqrt{\frac{\mu_1}{\epsilon_1}\frac{\mu_2}{\epsilon_2}}\,\tilde{\theta}^2$ and $\tilde{\theta} = \alpha\,\mathrm{sgn}(\Delta)\left(1 + \frac{\hbar^2 v_F^2}{12\Delta^2}k_0^2\right)$.

For incident light linearly polarized in the y direction, $\mathbf{E}_i = E_i^{\mathrm{TE}}\hat{\mathbf{e}}_y\, e^{i(k_z z - \omega t)}$, the Kerr and Faraday angles are defined by $\tan\theta_{\mathrm{K}} = (\mathbf{E}_r \cdot \hat{\mathbf{e}}_x)/(\mathbf{E}_r \cdot \hat{\mathbf{e}}_y)$, and $\tan\theta_{\mathrm{F}} = (\mathbf{E}_t \cdot \hat{\mathbf{e}}_x)/(\mathbf{E}_t \cdot \hat{\mathbf{e}}_y)$, respectively. Using the Fresnel matrix, we obtain

$$\tan\theta_{\mathrm{K}} \approx \frac{2\mu_2\sqrt{\epsilon_1\mu_1}}{\epsilon_1\mu_2 - \epsilon_2\mu_1}\alpha\,\mathrm{sgn}(\Delta)\left(1 + \mathcal{E}^2/3\right) + \mathcal{O}(\alpha^3) \tag{108}$$

and

$$\tan\theta_{\mathrm{F}} \approx \frac{1}{\sqrt{\epsilon_1/\mu_1} + \sqrt{\epsilon_2/\mu_2}}\alpha\,\mathrm{sgn}(\Delta)\left(1 + \mathcal{E}^2/3\right) + \mathcal{O}(\alpha^3), \tag{109}$$

respectively, where $\mathcal{E} \equiv \hbar\omega/2\Delta$ is the ratio between the photon energy and the bandgap. Now, we shall estimate the size of this effect in a realistic experimental situation. In Ref. [19], the authors reported the first experimental observation of the Faraday rotation angle when linearly polarized THz radiation passes through the surface of a strained HgTe 3D TI. They found a rotation angle of $\theta_{\mathrm{F}}^{(0)} \approx 7.3 \times 10^{-3}$ rad, within an error bar estimated at 0.1×10^{-3} rad. Using the experimental data of Ref. [19], with a photon energy of 1.4 meV, and an energy gap in strained HgTe of 10 meV [20], from Equation (109), one estimates a shift in the Faraday angle of

$$\delta\theta_{\mathrm{F}} = \theta_{\mathrm{F}} - \theta_{\mathrm{F}}^{(0)} = \arctan\left[\frac{(\mathcal{E}^2/3)\tan\theta_{\mathrm{F}}^{(0)}}{1 + (1 + \mathcal{E}^2/3)\tan^2\theta_{\mathrm{F}}^{(0)}}\right] \approx 1.2 \times 10^{-5}\mathrm{rad}, \tag{110}$$

which is on the verge of the current experimental accessibility (one order of magnitude below the experimental precision). This angle shift is strictly caused by the lowest-order derivative correction to the surface anomalous Hall effect.

We observe that correction (110) is driven by the parameter $\mathcal{E} \equiv \hbar\omega/2\Delta$, which is the ratio between the photon energy and the bandgap. If we increase this ratio, the angle shift could be enhanced in principle; however, the validity of the theory requires $\mathcal{E} \ll 1$ to avoid interband transitions. This prohibits the increment in the angle shift. Other TIs, such as $ZrTe_5$ crystals, exhibit a large energy gap of ∼100 eV, which implies $\delta\theta_{\mathrm{F}} \sim 4.6 \times 10^{-7}$ rad, which is three orders of magnitude below the error bars. All in all, strained HgTe is the best material candidate for testing our prediction.

6. Image Magnetic Monopole

The search for magnetic monopoles has a long history in both high-energy and condensed matter physics. Up to date, this elusive particle has yet to be detected experimentally. However, the development of topological insulators provides a new platform where these

kinds of magnetic excitations appear. To be precise, when the Fermi level lies within the bandgap, the surface Hall conductance is half-quantized and the electromagnetic response is described by axion electrodynamics with a quantized coefficient. If this condition is fulfilled, a point-like electric charge q near the surface of a topological insulator induces an image magnetic monopole charge of strength [21,22]

$$g = \frac{2q\alpha}{(\epsilon_1+\epsilon_2)(1/\mu_1+1/\mu_2)} + \mathcal{O}(\alpha^3). \tag{111}$$

If the Fermi level does not lie in the bandgap but lies within the finite density of states, the image monopole picture breaks down due to the screening effect [23]. As we shall see in the following, applying higher-order correction terms to the surface Hall effect also implies the breakdown of the image monopole picture, even when the Fermi level lies in the bandgap.

Let us consider the geometry as shown in Figure 5, where the left-half space ($z<0$) is occupied by a topological insulator, and the right-half space ($z>0$) is occupied by a trivial insulator. The interface, at $z=0$, supports a surface Hall conductivity $\sigma_{yx}(k)$ that includes derivative corrections. A point-like electric charge of strength q is located at a distance z_0 from the surface of a topological insulator. The field equations describing the electromagnetic response, including the surface Hall response, read

$$\nabla\cdot(\epsilon\mathbf{E}) = \rho(z) - \alpha\,\delta(z)\,\hat{\mathbf{n}}\cdot\hat{\mathcal{O}}_{\mathbf{r}_\perp}\,\mathbf{B}, \qquad \nabla\times(\mathbf{B}/\mu) = \alpha\,\delta(z)\,\hat{\mathbf{n}}\times\hat{\mathcal{O}}_{\mathbf{r}_\perp}\,\mathbf{E}, \tag{112}$$

where $\rho(z) = q\,\delta(z-z_0)$ and

$$\hat{\mathcal{O}}_{\mathbf{r}_\perp} = \mathrm{sgn}(\Delta)\left(1+\frac{\hbar^2 v_F^2}{12\Delta^2}\nabla_\perp^2\right), \tag{113}$$

when the chemical potential lies in the bandgap of the TI. Due to gauge invariance, the fields can be written in terms of the electromagnetic potentials according to $\mathbf{E} = -\nabla\phi$ and $\mathbf{B} = \nabla\times\mathbf{A}$, as usual. At the lowest order in α, the electromagnetic potentials are given by

$$\phi(\mathbf{r}) = \int G_\epsilon(\mathbf{r},\mathbf{r}')\,\rho(\mathbf{r}')\,d^3\mathbf{r}' + \mathcal{O}(\alpha^2), \tag{114}$$

$$\mathbf{A}(\mathbf{r}) = \alpha\int G_\mu(\mathbf{r},\mathbf{r}')\,\delta(z')\,\hat{\mathbf{n}}\times\hat{\mathcal{O}}_{\mathbf{r}'_\perp}\,\mathbf{E}(\mathbf{r}')\,d^3\mathbf{r}' + \mathcal{O}(\alpha^3), \tag{115}$$

in the Coulomb gauge, with the corresponding Green's functions

$$G_\epsilon(\mathbf{r},\mathbf{r}') = \frac{1}{4\pi\epsilon_1}\left[\frac{1}{\sqrt{|\mathbf{r}_\perp-\mathbf{r}'_\perp|^2+(z-z')^2}} + \frac{\epsilon_1-\epsilon_2}{\epsilon_1+\epsilon_2}\frac{1}{\sqrt{|\mathbf{r}_\perp-\mathbf{r}'_\perp|^2+(|z|+z')^2}}\right], \tag{116}$$

$$G_\mu(\mathbf{r},\mathbf{r}') = \frac{\mu_1}{4\pi}\left[\frac{1}{\sqrt{|\mathbf{r}_\perp-\mathbf{r}'_\perp|^2+(z-z')^2}} - \frac{\mu_1-\mu_2}{\mu_1+\mu_2}\frac{1}{\sqrt{|\mathbf{r}_\perp-\mathbf{r}'_\perp|^2+(|z|+z')^2}}\right]. \tag{117}$$

These potentials can be evaluated straightforwardly. On the one hand, the electric potential is exactly the same as in Maxwell electrodynamics, since time reversal dictates a quadratic correction in α, i.e.,

$$\phi(\mathbf{r}) = \frac{q}{4\pi\epsilon_1}\left[\frac{1}{\sqrt{r_\perp^2+(z-z_0)^2}} + \frac{\epsilon_1-\epsilon_2}{\epsilon_1+\epsilon_2}\frac{1}{\sqrt{r_\perp^2+(|z|+z_0)^2}}\right] + \mathcal{O}(\alpha^2), \tag{118}$$

which we interpret in terms of the original charge q at $z=z_0$ and an image electric charge of strength $q' = q\frac{\epsilon_1-\epsilon_2}{\epsilon_1+\epsilon_2}$ at $-z_0$, as usual. The magnetic part is a little more subtle. Time-

reversal symmetry implies a linear response in α, which we determine in the following. We observe that the integrand $\hat{\mathbf{n}} \times \hat{\mathcal{O}}_{\mathbf{r}'_\perp} \mathbf{E}(\mathbf{r}')$ depends on the transverse Laplacian acting upon the components of the electric field parallel to the interface, which are continuous there. Therefore, using the identity $\nabla_\perp G_\epsilon(\mathbf{r}, \mathbf{r}') = -\nabla'_\perp G_\epsilon(\mathbf{r}, \mathbf{r}')$, which is also valid for the magnetic Green's function $G_\mu(\mathbf{r}, \mathbf{r}')$, one can further present the identity

$$\int G_\mu(\mathbf{r}, \mathbf{r}')\, \delta(z')\, \hat{\mathbf{n}} \times \hat{\mathcal{O}}_{\mathbf{r}'_\perp} \mathbf{E}(\mathbf{r}')\, d^3\mathbf{r}' = \hat{\mathcal{O}}_{\mathbf{r}_\perp} \int G_\mu(\mathbf{r}, \mathbf{r}')\, \delta(z')\, \hat{\mathbf{n}} \times \mathbf{E}(\mathbf{r}')\, d^3\mathbf{r}'. \tag{119}$$

Therefore, the vector potential (115) can be written as $\mathbf{A}(\mathbf{r}) = \hat{\mathcal{O}}_{\mathbf{r}_\perp} \mathbf{A}^{(0)}(\mathbf{r})$, where

$$\mathbf{A}^{(0)}(\mathbf{r}) = -\alpha\, \hat{\mathbf{n}} \times \nabla \int G_\mu(\mathbf{r}, \mathbf{r}')\, \delta(z')\, \phi(\mathbf{r}')\, d^3\mathbf{r}', \tag{120}$$

and $\phi(\mathbf{r}')$ is the scalar potential (118). Straightforward calculations yield

$$\mathbf{A}^{(0)}(\mathbf{r}) = \frac{g}{4\pi} \frac{y\hat{\mathbf{e}}_x - x\hat{\mathbf{e}}_y}{r_\perp^2} \left[1 - \frac{|z| + z_0}{\sqrt{r_\perp^2 + (|z| + z_0)^2}} \right], \tag{121}$$

where g is given by Equation (111). We identify (121) as the vector potential of a straight vortex line or Dirac string over the z axis. The details of the calculations are relegated to Appendix F. The zeroth-order magnetic field can then be obtained by taking the curl of Equation (121), which yields the monopole field $\mathbf{B}^{(0)}(\mathbf{r}) = \frac{g}{4\pi} \frac{\mathbf{R}}{R^3}$, where $\mathbf{R} = \mathbf{r}_\perp + (|z| + z_0)\hat{\mathbf{e}}_z$. Taking the curl of the full vector potential, one finds the deviation from the magnetic monopole picture as

$$\delta\mathbf{B}(\mathbf{r}) = \mathbf{B}(\mathbf{r}) - \mathbf{B}^{(0)}(\mathbf{r}) = \left(\frac{\hbar v_F}{2\Delta z_0} \right)^2 \frac{z_0^2}{R^2} \left[\left(1 - 5\frac{(|z| + z_0)^2}{R^2} \right) \hat{\mathbf{I}} + 2\hat{\mathbf{e}}_z \hat{\mathbf{e}}_z \right] \cdot \mathbf{B}^{(0)}(\mathbf{r}), \tag{122}$$

where $\hat{\mathbf{I}}$ is the unit dyadic.

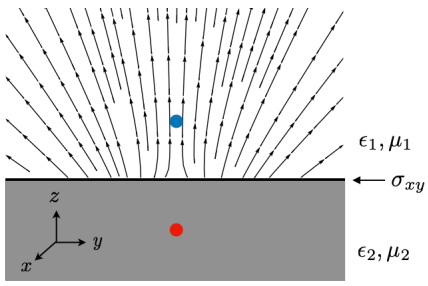

Figure 5. Plot of the total magnetic field $\mathbf{B}(\mathbf{r})$ due to a point-like electric charge (marked in blue) above the topological insulator HgTe.

In Figure 5, we plot the total magnetic field $\mathbf{B}(\mathbf{r})$ due to a point-like electric charge (marked in blue) above the topological insulator. The field strength is normalized by the magnetic field strength $B_0 = g/4\pi z_0^2$. If solely the Hall conductivity is taken into account, the magnetic field lines above the surface are radially directed away from a magnetic monopole located beneath the surface (marked in red). However, in the present case, as we can see in Figure 5, the monopole picture breaks down, since the magnetic field lines are no longer radially directed from the image point. The deviations in the field lines are apparent near the surface, while the radial behavior dominates at long distances. Our results show that, when the Fermi level lies within the gap, the image monopole picture emerges only as first-order in the electromagnetic response. Higher-order corrections yield to deviations from the magnetic monopole field.

Now, we shall estimate the size of this effect. For an electric charge of strength $q = 200e$ (where e is the elementary charge) in vacuum, located at a distance $z_0 = 2$ µm from the TI surface and in taking $\mu_2 = \mu_0$ and $\epsilon_2 = 20\epsilon_0$, the magnetic field at an observation point at $z = 600$ µm away is $B^{(0)} = 0.921$ pT [24], which is too small to be detected directly in an experiment. For a strained HgTe, for which $\Delta = 10$ meV and $v_F = 5 \times 10^5$ m/s, Equation (122) predicts $\delta B = 3 \times 10^{-7} B^{(0)}$, which is seven orders of magnitude below the uncorrected prediction. With the present experimental precision, this field and its correction cannot be observed [25]. However, as shown recently in Ref. [24], integrating TIs with active metamaterials substrates can enhance the induced monopole magnetic field $B^{(0)}$ by more than 10^4 times, and in our case, the correction term as well, which is proportional to $B^{(0)}$. This idea opens a new avenue for the search of the elusive monopole field and represents an interesting possibility with which to test our results as well.

7. Summary and Conclusions

The main goal of this work was to obtain higher-order corrections in the derivatives for the electromagnetic response of topological insulators (TIs) at zero temperature at finite density. The focus was on the anomalous Hall conductivity σ_{yx}, which governs the electromagnetic response of the TI at the interface. We recover the known zeroth-order results for σ_{yx} using both the linearized Kubo approximation and the semi-classical Boltzmann method, which incorporates anomalous transport through the inclusion of the Berry phase. Unfortunately, both methods are not capable of incorporating higher-order corrections in the derivatives in their current formulation. For this reason, we consider a third alternative based on the calculation of radiative corrections in quantum electrodynamics encoded in the vacuum polarization tensor.

We proceed in two steps, recalling that the electromagnetic behavior of topological insulators under the given conditions is well described by axion electrodynamics, with a constant piecewice axion parameter having a discontinuity at the interface, as shown in Figure 1. To begin with, and in order to maintain the basic structure of the underlying axion electrodynamics, we propose an extension that consistently includes these corrections in the surface current K^μ that appears at the interface of the media. At this level, the most important result is presented in Equations (27) and (28), where K^μ is written in terms of differential operators in the transverse coordinates to the interface acting on the fields. This current derives from the modified axion electrodynamics in a way analogous to the standard case since the transverse operators are still localized at the interface. In momentum space, the resulting Hall conductivity is given by Equation (28) and constitutes a direct generalization of the standard expression (5) in terms of the newly introduced transverse operators.

The second step includes the calculation of the corrections themselves, which are naturally obtained from the radiative corrections in the coupling of fermions at the interface of the materials with the electromagnetic field described by (2 + 1)D electrodynamics. In general terms, we calculate the resulting effective electromagnetic action at the (2 + 1)D interface, which is encoded in the transverse contribution of the vacuum polarization tensor $\Pi^{\mu\nu}$ to one-loop order, which is proportional to $\epsilon^{\mu\nu\rho}$. Gauge invariance provides the tensorial structure of $\Pi^{\mu\nu}$, which is finally characterized by the scalar $\Pi_T(k)$, which contains the momentum corrections. From Equations (28) and (45), we obtain the relation $\sigma_{yx}(k) = \frac{e^2}{2}\Pi_T(k)$ that connects the response in axion electrodynamics with the radiative corrections at the interface from where the corrections in momentum arise. Appendix A includes a heuristic review of the derivation of the electromagnetic effective action together with additional references.

$\Pi_T(k)$ is calculated using the derivative expansion method, which provides the local contributions to the effective action in a power series of the external momentum. With this approach, one can also select from the very beginning the required order in the series expansion. Given that the anomalous Hall effect critically depends on the position of the Fermi level μ relative to the energy gap, we took into account its dependence on the calculation of σ_{yx} by applying the Matsubara extension to the final expression of the VPT at zero temperature. The results are indicated in Equations (85) and (86) for μ inside the bangap and for μ outside the bandgap, respectively. The corresponding expressions in terms of the anomalous Hall conductivity are given by Equations (90) and (91), with corrections up to the second order in the momentum.

For greater clarity, we included Appendix B, where we provide a brief summary of the derivative expansion method, along with references [26–36], which correspond to other works that have utilized this method. The main identity of the derivative expansion is given in Equation (51), while the explicit expansion is shown in Equation (60). Additionally, Appendices C–E contain detailed steps for calculating integrals and residues, which allowed us to derive the results presented in the manuscript for the polarization tensor at both zero and finite chemical potential.

As shown in Equations (28) and (30), the values for σ_{yx} determine the boundary conditions for the electromagnetic fields at the interface between two topological insulators. Keeping this in mind, we examine the implications of the calculated corrections on two well-established phenomena: firstly, the Kerr and Faraday rotations that occur when an electromagnetic wave impinges on the interface, and secondly, the ensuing magnetoelectric effect that arises when a charge is located in front of the interface.

In the first scenario, we examine an electromagnetic wave incident upon the topological insulator interface in the xz-plane, as depicted in Figure 4. By applying the boundary conditions (100), we compute reflection matrix (104) and transmission matrix (106), thereby deriving the Kerr and Faraday angles expressed in (108) and (109) for the specific case of normal incidence and for linearly polarized light in the y direction. In Ref. [19], the authors reported the first experimental observation of the Faraday rotation angle when linearly polarized THz radiation passes through the surface of a strained HgTe 3D TI. They found a rotation angle of $\theta_{\mathrm{F}}^{(0)} \approx 7.3 \times 10^{-3}$ rad, within an error bar estimated at 0.1×10^{-3} rad. Using the experimental data of Ref. [19], with a photon energy of 1.4 meV and an energy gap in strained HgTe of 10 meV [20], from Equation (109), we estimate the shift in the Faraday angle $\delta\theta_{\mathrm{F}} = \theta_{\mathrm{F}} - \theta_{\mathrm{F}}^{(0)} \approx 1.2 \times 10^{-5}$ rad, which is on the verge of the current experimental accessibility, just one order of magnitude below the experimental precision. This angle shift is strictly caused by the lowest-order derivative correction to the surface anomalous Hall effect.

The second scenario pertains to a notable manifestation of the magnetoelectric effect in TIs, wherein the placement of an electric charge in proximity to the TI interface gives rise to the appearance of an image magnetic monopole. To be precise, when the Fermi level lies within the bandgap, the surface Hall conductance is half-quantized and the image magnetic monopole is induced [21,22] However, when the Fermi level lies within the finite density of states, the image monopole picture breaks down due to the screening effect [23]. We examined the implications of the Fermi level being situated within the energy gap, while σ_{yx} incorporates the momentum corrections specified in Equation (113), and found that the resultant magnetic field can no longer be interpreted in terms of an image monopole. The calculation is carried out to the first order in α and involves the derivative corrections produced by the operator $\hat{\mathcal{O}}_{\mathbf{r}_\perp}$ in Equation (113), which determines the vector potential in Equation (108) that can be rewritten as $\mathbf{A}(\mathbf{r}) = \hat{\mathcal{O}}_{\mathbf{r}_\perp}\mathbf{A}^{(0)}(\mathbf{r})$. Here, $\mathbf{A}^{(0)}$ is the vector potential of a straight Dirac string over the z axis yielding the original monopole field

$\mathbf{B}^{(0)}(\mathbf{r}) = \frac{g}{4\pi}\frac{\mathbf{r}}{r^3}$. The shift $\delta\mathbf{B}(\mathbf{r}) = \mathbf{B}(\mathbf{r}) - \mathbf{B}^{(0)}(\mathbf{r})$ is reported in Equation (122), and the total magnetic field $\mathbf{B}$ is plotted in Figure 5. We see that the monopole picture breaks down, since the magnetic field lines are no longer radially directed from the image point. The deviations in the field lines are apparent near the surface, while the radial behavior dominates at long distances. Our results show that, even when the Fermi level lies within the gap, the image monopole picture emerges only at the zeroth-order momentum correction in the electromagnetic response. Higher-order corrections yield to deviations from the magnetic monopole field.

Some final comments now emphasize how our findings differ and extend the results of previous models addressing non-local corrections in non-dynamical axion electrodynamics, which are relevant to topological insulators and Weyl semimetals. These corrections can be embedded in the general higher-derivative electromagnetic Lorentz-violating modifications to Maxwell's equations, as discussed in Refs. [37,38], for example. However, this phenomenological approach does not necessarily result from the effective electromagnetic response of an underlying fermionic system. While the calculation of effective electromagnetic actions in field theory has a long history and has been used in many applications, here, we focused on the above-mentioned cases relevant to condensed matter physics. In the case of the Weyl semimetals, for example, the focus is on the electromagnetic response of the bulk, and two possibilities arise: modifying Maxwell's equations directly in a phenomenological way and deriving the electromagnetic response from the full fermionic $(3+1)$-D system coupled to the electromagnetic field. The latter approach yields modifications to Maxwell's equations through radiative corrections of the effective action, including the vacuum polarization tensor in the one-loop approximation [12,13,39]. For topological insulators, the corresponding axion ED introduces new dynamical effects only at the $(2+1)$-D interface between two media. The bulk is still described by standard Maxwell's equations. Most higher-order derivative corrections in the literature focus on modifying only the electromagnetic $2+1$-D theory at the boundary in a phenomenological way, as, for example, in Ref. [40]. An additional example of an alternative phenomenological proposal for a modified axion ED, this time in the bulk, is found in Ref. [10]. Additionally, we account for effects due to the inclusion of the chemical potential, which are not considered in these studies. Our approach focuses on the $(2+1)$-D full fermionic system coupled to the electromagnetic field, and proceeds by calculating higher-order derivative corrections to the anomalous Hall conductivity arising from the one-loop correction to the corresponding effective electromagnetic action via the vacuum polarization tensor. We also establish a link between the theory at the boundary and at the bulk, obtaining a well-motivated modified version of the axion ED for this case.

Author Contributions: Conceptualization, R.M.v.D., A.M.-R. and L.F.U.; Investigation, R.M.v.D., A.M.-R. and L.F.U.; Writing – original draft, R.M.v.D., A.M.-R. and L.F.U. All authors have read and agreed to the published version of the manuscript.

Funding: This research received no external funding.

Data Availability Statement: All data generated or analyzed during this study are included in this published article.

Acknowledgments: R.M.v.D., A.M.-R., and L.F.U. were partially supported by DGAPA-UNAM Project No. AG100224 and by Project CONACyT (México) No. 428214. R.M.v.D. was supported by the DGAPA-UNAM Posdoctoral Program. A.M.-R. acknowledges the support provided by the Marcos Moshinsky Foundation.

Conflicts of Interest: The authors declare no conflicts of interest.

Abbreviations

The following abbreviations are used in this manuscript:

VPT	Vacuum polarization tensor;
TI	Topological insulator;
TR	Time reversal;
DOS	Density of states;
TR	Time-reversal symmetry;
THz	Tera Hertz;
TE	Transversal electric;
TM	Transversal magnetic;
SME	Standard model extension.

Appendix A. Heuristic Calculation of the Path Integral Yielding the Effective Action

Quantum electrodynamics (QEDs) are traditionally described using Feynman diagrams, which arise from the canonical quantization of the Dirac and electromagnetic fields yielding the corresponding operators. These diagrams lend themselves to a particle interpretation and provide a pictorial representation of the amplitude for a given process. The interaction vertex $e\bar{\Psi}\gamma^\mu\Psi A_\mu$, combined with fermion and photon propagators, yields the numerical value of the amplitude using the derived Feynman rules. An alternative quantization method that offers a more compact and systematic formulation is based on a path integral representation of the matrix elements of the evolution operator. This operator connects initial and final states, conveniently chosen as the ground state of the system at $t \to -\infty$ and $t \to +\infty$, respectively. This approach yields the vacuum-to-vacuum amplitude,

$$\langle 0_+|0_-\rangle_{\eta,\bar{\eta},J} = \int \mathcal{D}A\,\mathcal{D}\bar{\psi}\,\mathcal{D}\psi\; e^{\frac{i}{\hbar}\int d^4x\left(\mathcal{L}_\Psi(\bar{\Psi},\Psi,A)+\mathcal{L}(A)+\mathcal{L}_{\mathrm{gf}}+\bar{\eta}\Psi+\bar{\Psi}\eta+J^\mu A_\mu\right)} \tag{A1}$$

which contains all the required correlation functions to calculate arbitrary processes in the full theory. Here, we include the full action of the theory by adding the Lagrangian of the electromagnetic field $\mathcal{L}(A)$ plus a gauge-fixing term $\mathcal{L}_{\mathrm{gf}}$, together with the external sources $\bar{\eta}, \eta$, and J^μ. Let us emphasize that in this formulation, all the fields and sources are either complex numbers or Grassman numbers, instead of operators. When examining the quantum response of a fermionic system to an external classical electromagnetic field, the problem simplifies significantly. This is because the path integral over $\mathcal{D}A$ is no longer required. The primary focus now shifts to calculating the effective electromagnetic action $S\mathrm{eff}[A]$ defined by

$$e^{iS_{\mathrm{eff}}[A]/\hbar} = \int \mathcal{D}\bar{\psi}\,\mathcal{D}\psi\; e^{\frac{i}{\hbar}\int d^4x\,\mathcal{L}_\Psi} \tag{A2}$$

This action is added to the standard electromagnetic action, yielding the modified Maxwell equations that describe the electromagnetic response of the medium.

The next step is to assign an operational meaning to the integration in Equation (A2), which solely involves fermionic fields. However, this poses an additional complication due to the Fermi–Dirac statistics, which dictate that two fermions cannot occupy the same quantum state. In the operator formulation, this translates to the creation (annihilation) operators with zero square, thereby defining an anticommutator algebra. In the path integral formulation, this property is realized by introducing a real Grassmann number basis $\{\bar{a}_n,\, a_n\}, n = 1 \ldots N$. By definition, any two Grassmann numbers anticommute, implying that every Grassmann number has zero square. This property enables the correct representation of fermionic fields within the path integral framework. Also, Grassmann numbers

and complex numbers commute among each other, and any product of an even number of Grassmann numbers behaves like another complex number regarding commutative properties. Most importantly, the integration properties are

$$\int d\bar{a}_n = 0, \qquad \int da_n = 0, \qquad \int d\bar{a}_n \bar{a}_m = \delta_{nm}, \qquad \int da_n a_m = \delta_{nm}, \tag{A3}$$

where any two differentials anticommute among themselves and with any other Grassman number. Also, the full measure is defined as

$$\mathcal{D}\bar{\psi}\,\mathcal{D}\psi = \prod_n (da_n\, d\bar{a}_n) \tag{A4}$$

Now, let us consider the following integration:

$$I = \int \mathcal{D}\bar{\psi}\,\mathcal{D}\psi\ \exp\left\{\frac{i}{\hbar}\int d^4x \left(\Psi^\dagger(x)\hat{O}_x\Psi(x)\right)\right\} \tag{A5}$$

where $\hat{O}_x$ is a Hermitian matrix-valued differential operator in the variable x, which reduces to

$$\hat{O}_x = \gamma_0\Big[v_F(i\hbar\not{\partial} + e\not{A}) - \Delta\Big] \tag{A6}$$

in the case of the effective action calculation. Since $\hat{O}_x$ is Hermitian, it has real eigenvalues λ_i and a complete set of orthonormal matrix-valued complex eigenfuntions $\Phi_i(x)$ such that

$$\hat{O}_x\Phi_n(x) = \lambda_n\,\Phi_n(x), \qquad \int d^4x\,\Phi_n^\dagger(x)\Phi_m(x) = \delta_{nm} \tag{A7}$$

Naively, a path integral can be viewed as an integration over all possible configurations of the fields, which we now label by expanding each field in the Grassmann basis as

$$\Psi(x) = \sum_n a_n\Phi_n(x), \qquad \Psi^\dagger(x) = \sum_n \bar{a}_n\Phi_n^\dagger(x). \tag{A8}$$

Substituting this expansions in the exponential factor of integral (A5), and after successive steps, we obtain

$$\begin{aligned}\exp\left\{\frac{i}{\hbar}\int d^4x \left(\Psi^\dagger(x)\hat{O}_x\Psi(x)\right)\right\} &= \exp\left\{\frac{i}{\hbar}\sum_{m=1}^{N}\left(\bar{a}_m a_m\lambda_m\right)\right\} = \prod_{m=1}^{N}\left(\exp\frac{i}{\hbar}\bar{a}_m a_m\lambda_m\right)\\ &= \prod_{m=1}^{N}\left(1+\frac{i}{\hbar}\bar{a}_m a_m\lambda_m\right).\end{aligned} \tag{A9}$$

Among other properties, in the last step, we use that $\exp(1+z) = 1+z$ whenever $z^2 = 0$. Now, we are ready to take integral (A5) using measure (A4), which includes all the Grassman variables forming the basis. Consequently, following the integration rules defined in (A3), the only terms that survives in product (A9) is also that containing all contributions $\bar{a}_m a_m$:

$$I = \left(\frac{i}{\hbar}\right)^N \int \prod_n (da_n\, d\bar{a}_n)(\bar{a}_1 a_1\lambda_1)(\bar{a}_2 a_2\lambda_2)\ldots(\bar{a}_N a_N\lambda_N). \tag{A10}$$

In the last step, every factor $\bar{a}_i a_i\lambda_i$ can be moved next to the corresponding diferential yielding $\int (da_i\, d\bar{a}_i)\,\bar{a}_i a_i\lambda_i = \lambda_i$, yielding the final result

$$\int \mathcal{D}\bar{\psi}\,\mathcal{D}\psi\ \exp\left\{\frac{i}{\hbar}\int d^4x \left(\Psi^\dagger(x)\hat{O}_x\Psi(x)\right)\right\} = \left(\frac{i}{\hbar}\right)^N \prod_{n=1}^{N}\lambda_n = \left(\frac{i}{\hbar}\right)^N \det\hat{O}, \tag{A11}$$

where we have identified the product of the eigenvalues of the operator $\hat{O}$ as its determinant, which can be subsequently calculated using any alternative method. From the definition of the effective action (A2), we realize that the relevant contribution is $\ln\left(\left(\frac{i}{\hbar}\right)^N \det\hat{O}\right) = N\ln\frac{i}{\hbar} + \ln\det\hat{O}$ such that the factor $\left(\frac{i}{\hbar}\right)^N$ is irrelevant. Going back to the effective action, the final answer is

$$S_{\text{eff}}[A] = -i\hbar\ln\det[v_F(\hbar\not{p} + e\not{A}) - \Delta], \tag{A12}$$

which can be presented as Equation (48) in the manuscript after employing the identity

$$\ln\det\hat{O} = \text{Tr}\ln\hat{O}. \tag{A13}$$

For a detailed review, see, for example, the following texts on quantum field theory: [41,42].

Appendix B. The Derivative Expansion

This method was introduced in Refs. [26–28], and many applications have been put forward for different topics, such as the chiral anomaly [29,30]; the radiative induction of the Chern–Simons term in (2 + 1) dimensions [31] and its higher-derivative counterpart [32]; and the calculation of radiative corrections in the SME [43], as shown, for example, in Refs. [33–36]. In this appendix, we briefly review the main steps of the method in the one-dimensional case, which can nevertheless be generalized to arbitrary dimensions in a straightforward manner.

The method provides an alternative way for calculating traces of products of momentum- and coordinate-dependent operators. The operation Tr includes traces in coordinate (momentum) space, as well as traces in a matrix space. To be precise, we deal with objects like

$$T^{(n)} \equiv \text{Tr}\Big(M_1(\hat{p})C_1(\hat{x})\, M_2(\hat{p})C_2(\hat{x})\ldots M_n(\hat{p})C_n(\hat{x})\Big), \tag{A14}$$

where $\hat{x}$ and $\hat{p}$ denote coordinate and momentum operators with standard commutation relations $[\hat{x},\hat{p}] = -i$, and with $\hat{p} = id/dx$ in the coordinate representation. We assume that each $\hat{p}$-dependent function in (A14) can be expanded in a power series of the argument, while we deal with the exact expressions for the $\hat{x}$-dependent functions. The basic idea is to use the basic commutation relation to rearrange expression (A14) in such a way that it can be written as a sum of terms, where, by convention, the momentum operators are written to the left and the coordinate operators are written to the right:

$$T^{(n)} = \sum_N T_N^{(n)} \equiv \sum_N \text{Tr}\Big(L_N^{(n)}(\hat{p})\, R_N^{(n)}(\hat{x})\Big). \tag{A15}$$

Once this is achieved, each contribution N to the full trace can be immediately calculated as

$$\begin{aligned} T_N^{(n)} &= \text{tr}\int dx\langle x|L_N^{(n)}(\hat{p})\, R_N^{(n)}(\hat{x})|x\rangle = \int dx\langle x|L_N^{(n)}(\hat{p})|x\rangle\, R_N^{(n)}(\,x) \\ &= \text{tr}\int dx\int\frac{dp}{(2\pi)}\, L_N^{(n)}(\,p)\, R_N^{(n)}(x) \end{aligned} \tag{A16}$$

in terms of the numerical functions $L_N(p)$ and $R_N(x)$. The notation tr indicates a remaining trace in a matrix space. We are using the standard scalar product $\langle x|p\rangle = e^{-ipx}/\sqrt{2\pi}$ together with the completeness of each orthonormal basis.

Let us consider the simplest situation:

$$T^{(2)} = \mathrm{Tr}\Big(M_1(\hat{p})C_1(\hat{x})\, M_2(\hat{p})C_2(\hat{x})\Big) \tag{A17}$$

where we need to interchange C_1 and M_2. Assuming M_2 has a power expansion in $\hat{p}$, we examine the contributions of $\hat{p}^n$ to the commutator $[C_1(\hat{x}), M_2(\hat{p})]$. We start from the basic commutator $[C_1(\hat{x}), \hat{p}]$, which we reorganize into the convenient form

$$C_1(\hat{x})\,\hat{p} = \Big(\hat{p} - i\frac{d}{d\hat{x}}\Big)C_1(\hat{x}). \tag{A18}$$

To firmly establish the notation and the conventions, we calculate the next contribution:

$$[C_1(\hat{x}), \hat{p}^2] \quad = \quad -2i\hat{p}\frac{dC_1(\hat{x})}{d\hat{x}} - \frac{d^2C_1(\hat{x})}{d\hat{x}^2}, \tag{A19}$$

where we choose to write the $\hat{p}$ operators to the left and the $\hat{x}$ operators to the right, according to our convention. Next, we identify the term $C_1(\hat{x})\hat{p}^2$ as

$$C_1(\hat{x})\hat{p}^2 = \Big(\hat{p}^2 - 2i\hat{p}\frac{d}{d\hat{x}} - \frac{d^2}{d\hat{x}^2}\Big)C_1(\hat{x}). \tag{A20}$$

This is an exact operator expression, and Equation (A19) makes it clear that $\frac{d}{d\hat{x}}$ acts only in the operator C_1. A crucial step in the notation arises after rewriting the operator on the right-hand side of Equation (A20) is

$$\Big(\hat{p}^2 - 2i\hat{p}\frac{d}{d\hat{x}} - \frac{d^2}{d\hat{x}^2}\Big) = \Big(\hat{p} - i\frac{d}{d\hat{x}}\Big)^2. \tag{A21}$$

In other words, from now on, we are assuming that the operator $\hat{p}$ commutes with $\frac{d}{d\hat{x}}$, which naturally acts to the right on the corresponding $C_1(\hat{x})$. That is to say, $\frac{d}{d\hat{x}}$ will be considered a C-number in the following. Having established this convention, we immediately obtain the relations

$$C_1(\hat{x})\hat{p}^n = \Big(\hat{p} - i\frac{d}{d\hat{x}}\Big)^n C_1(\hat{x}), \tag{A22}$$

obtained by multiplying the $(n-1)$ equation to the left by $\hat{p}$ and using (A18). With the use of the power expansion of $M_2(\hat{p})$, this yields

$$C_1(\hat{x})M_2(\hat{p}) = M_2\Big(\hat{p} - i\frac{d}{d\hat{x}}\Big)C_1(\hat{x}). \tag{A23}$$

Here, we recall that the derivative $\frac{d}{d\hat{x}}$ acts only upon the exchanged operator C_1.

To make explicit the remaining step in the method, let us consider $T^{(3)}$, for example,

$$T^{(3)} = \mathrm{Tr}\Big(M_1(\hat{p})\Big[C_1(\hat{x})\, M_2(\hat{p})C_2(\hat{x})\, M_3(\hat{p})\Big]C_3(\hat{x})\Big), \tag{A24}$$

and focus on the term in square brackets:

$$\Big[\Big(C_1(\hat{x})\, M_2(\hat{p})\Big)\Big(C_2(\hat{x})M_3(\hat{p})\Big)\Big] = M_2\Big(\hat{p} - i\frac{d}{d\hat{x}_1}\Big)\Big[C_1(\hat{x})\; M_3\Big(\hat{p} - i\frac{d}{d\hat{x}_2}\Big)\Big]C_2(\hat{x}), \tag{A25}$$

where we use prescription (A23) to move C_1 through M_2 and C_2 through M_3. We labeled the derivatives as $\frac{d}{d\hat{x}_i}$ to make sure that that they only act upon the corresponding $C_i(\hat{x})$. We still have to move $C_1(\hat{x})$ across $M_3(\hat{p})$ in order to have all $\hat{x}$-dependent operators to

the right. Recalling $\frac{d}{d\hat{x}_2}$ is a commuting object, we define $\hat{P} = \hat{p} - i\frac{d}{d\hat{x}_2}$, which satisfies $[\hat{x}, \hat{P}] = -i$, as in our initial commutation relation. Then, following the previous steps, we obtain

$$C_1(\hat{x})M_3(\hat{P}) = M_3\Big(\hat{P} - i\frac{d}{dx_1}\Big)C_1(\hat{x}) = M_3\Big(\hat{p} - i\frac{d}{dx_2} - i\frac{d}{dx_1}\Big)C_1(\hat{x}), \tag{A26}$$

after substituting back $\hat{P}$.

Summarizing, we have

$$T^{(3)} = \mathrm{Tr}\Big(M_1(\hat{p})M_2\Big(\hat{p} - i\frac{d}{d\hat{x}_1}\Big)M_3\Big(\hat{p} - i\frac{d}{d\hat{x}_2} - i\frac{d}{d\hat{x}_1}\Big)C_1(\hat{x})C_2(\hat{x})C_3(\hat{x}).\Big) \tag{A27}$$

Since the product of M_1, M_2, and M_3 involves only the operator $\hat{p}$ together with commuting objects $\frac{d}{d\hat{x}_i}$ and because all operators $C_i(\hat{x})$ have been moved to the right, $T^{(3)}$ has just the form indicated in Equation (A16), yielding the final value

$$T^{(3)} = \mathrm{tr}\int \frac{dp}{(2\pi)}dx\Big(M_1(p)M_2\Big(p - i\frac{d}{dx_1}\Big)M_3\Big(p - i\frac{d}{dx_2} - i\frac{d}{dx_1}\Big)C_1(x)C_2(x)C_3(x)\Big). \tag{A28}$$

The generalization to higher dimensions is direct with $[\hat{x}^\mu, \hat{p}_\nu] = -i\delta^\mu{}_\nu$. In the case of Equation (A23), we obtain the relation $A(\hat{x}^\mu)S(\hat{p}^\nu) = S(\hat{p}_\nu - i\partial_\nu)A(\hat{x}^\mu)$, which is frequently used in this manuscript.

Another example is the extension of $T^{(3)}$:

$$\begin{aligned} T^{(3)} &= \mathrm{Tr}\big[M_1(\hat{p}_\mu)C_1(\hat{x}^\nu)\, M_2(\hat{p}_\mu)\big(C_2(\hat{x}^\nu)M_3(\hat{p}_\mu)\big)C_3(\hat{x}^\nu)\big] \\ T^{(3)} &= \mathrm{Tr}\Big(M_1(\hat{p}_\mu)M_2\Big(\hat{p}_\nu - i\frac{\partial}{\partial\hat{x}_1^\nu}\Big)M_3\Big(\hat{p}_\rho - i\frac{\partial}{\partial\hat{x}_2^\rho} - i\frac{\partial}{\partial\hat{x}_1^\rho}\Big)C_1(\hat{x}^\alpha)C_2(\hat{x}^\beta)C_3(\hat{x}^\gamma).\Big) \end{aligned} \tag{A29}$$

which we finally evaluate as

$$T^{(3)} = \int \frac{d^4p}{(2\pi)^4}d^4x\Big(M_1(p_\mu)M_2\Big(p_\nu - i\frac{\partial}{\partial x_1^\nu}\Big)M_3\Big(p_\rho - i\frac{\partial}{\partial x_2^\rho} - i\frac{\partial}{\partial x_1^\rho}\Big)C_1(x^\alpha)C_2(x^\beta)C_3(x^\gamma)\Big). \tag{A30}$$

in terms of numerical functions.

The final goal of effective action calculations is to obtain a local function of x inside the d^4x integral, which yields the effective Lagrangian. The standard strategy is to expand the functions M_i by the powers of the derivatives times the functions of the momentum, which explains the name of "the derivative expansion" given to the method. The general form of the resulting expression is

$$T^{(3)} = \int \frac{d^4p}{(2\pi)^4}d^4x\Big(N_0 + N_1^\mu(p)\partial_\mu + N_2^{\mu\nu}(p)\partial_\mu\partial_\nu + \cdots\Big)C_1(x)C_2(x)C_3(x). \tag{A31}$$

p-integration can now be performed on each term, thus providing a dependence upon the additional parameters of the model, and the gradient operators end up acting upon the respective functions $C_i(x)$, yielding a local dependence on $C_i(x)$ and their derivatives.

Appendix C. Evaluation of the Function $I_\alpha^\beta(m)$

In Section 4.3, we introduced the function $I_\alpha^\beta(m)$, defined by Equation (84), to evaluate the VPT at zero chemical potential. In this section, we evaluate the integral in detail. To

this end, we first consider the Euclidean space through a Wick rotation given by $p_0 \to ip_0$, such that $p^2 \to -p^2$. Therefore, the integral given by Equation (84) becomes

$$I_\alpha^\beta(m) = i\,(-1)^{\alpha+\beta} \int \frac{d^3p}{(2\pi)^3}\,\frac{p^{2\beta}}{(p^2+m^2)^\alpha}. \tag{A32}$$

Introducing spherical coordinates, we obtain

$$I_\alpha^\beta(m) = i\,\frac{(-1)^{\alpha+\beta}}{(2\pi)^3}\int_0^{2\pi} d\phi \int_0^{\pi} d\theta\,\sin\theta \int_0^\infty dp\,\frac{p^{2(\beta+1)}}{(p^2+m^2)^\alpha}, \tag{A33}$$

and given the spherical symmetry of the integrand, one can directly integrate the angular variables, thus obtaining

$$I_\alpha^\beta(m) = i\,\frac{(-1)^{\alpha+\beta}}{2\pi^2}\int_0^\infty dp\,\frac{p^{2(\beta+1)}}{(p^2+m^2)^\alpha}. \tag{A34}$$

This integral seems somewhat familiar, but not quite. We can present it in a more familiar form by introducing the change in variables $p^2 = xm^2$, such that $2\sqrt{x}|m|dp = m^2dx$. Therefore, we obtain

$$\begin{aligned} I_\alpha^\beta(m) &= i\,\frac{(-1)^{\alpha+\beta}}{4\pi^2}\int_0^\infty \frac{|m|\,dx}{\sqrt{x}}\,x^{\beta+1}\,|m|^{2(\beta+1)}\left(x|m|^2+|m|^2\right)^{-\alpha} \\ &= i\,\frac{(-1)^{\alpha+\beta}}{4\pi^2}\,|m|^{-2\alpha+2\beta+3}\int_0^\infty dx\,x^{\beta+\frac{3}{2}-1}(x+1)^{-\alpha}. \end{aligned} \tag{A35}$$

The integral in x encloses an integral representation of the Beta function, given by

$$B(\gamma,\lambda) = \int_0^\infty dx\,x^{\gamma-1}\,(x+1)^{-\gamma-\lambda} = \frac{\Gamma(\gamma)\Gamma(\lambda)}{\Gamma(\gamma+\lambda)}. \tag{A36}$$

With this definition, the required integral becomes

$$I_\alpha^\beta(m) = i\,\frac{(-1)^{\alpha+\beta}}{4\pi^2}\,|m|^{-2\alpha+2\beta+3}\,B\left(\beta+\frac{3}{2},\alpha-\beta-\frac{3}{2}\right). \tag{A37}$$

From this general expression, one can evaluate the integrals required in Section 4.3, which are

$$I_2^0(m) = \frac{i}{8\pi|m|}, \qquad I_3^0(m) = -\frac{i}{32\pi|m|^3}, \qquad I_4^1(m) = -\frac{i}{64\pi|m|^3}. \tag{A38}$$

Substituting these results into Equation (70), we establish the final result given by Equation (72).

Appendix D. Calculation of the Residues

In this section, we compute the residues of the functions discussed in Section 4.4. To this end, we recall the limit formula for higher-order poles. If p_0^* is a pole of order n, then the residue of $F(p_0,\mathbf{p})$ around $p_0 = p_0^*$ can be found using the following formula:

$$\mathrm{Res}[F(p_0,\mathbf{p}), p_0 = p_0^*] = \frac{1}{(n-1)!}\lim_{p_0\to p_0^*}\left\{\frac{d^{(n-1)}}{dp_0^{(n-1)}}\left[(p_0-p_0^*)^n\,F(p_0,\mathbf{p})\right]\right\}. \tag{A39}$$

First, we calculate the residue for the function $g^{(2)}(p_0, \mathbf{p})$, i.e.,

$$\begin{aligned}\mathrm{Res}[g^{(2)}(p_0, \mathbf{p}), p_0 = p^*_{0s}] &= \lim_{p_0 \to p^*_{0s}} \left\{ \frac{d}{dp_0} \left[(p_0 - p^*_{0s})^2 \, \frac{1}{(p_0 - p^*_{0s})^2 \, (p_0 + p^*_{0s})^2} \right] \right\} \Big|_{p_0 = p^*_{0s}} \\ &= -\frac{2}{(p^*_{0s} + p^*_{0s})^3} = -\frac{s}{(|\mathbf{p}|^2 + m^2)^{3/2}},\end{aligned} \tag{A40}$$

where we used that $p^*_{0s} = s\sqrt{|\mathbf{p}|^2 + m^2}$ with $s = \pm 1$. One can calculate the residue for the function $g^{(3)}(p_0, \mathbf{p})$ in a similar manner. We find

$$\begin{aligned}\mathrm{Res}[g^{(3)}(p_0, \mathbf{p}), p_0 = p^*_{0s}] &= \frac{1}{2} \lim_{p_0 \to p^*_{0s}} \left\{ \frac{d^2}{dp_0^2} \left[(p_0 - p^*_{0s})^3 \, \frac{1}{(p_0 - p^*_{0s})^3 \, (p_0 + p^*_{0s})^3} \right] \right\} \\ &= \frac{6}{(p^*_{0s} + p^*_{0s})^5} = \frac{3s}{16(|\mathbf{p}|^2 + m^2)^{5/2}}.\end{aligned} \tag{A41}$$

Finally, we compute the residue of the function $f^{(4)}_{\lambda\sigma}(p_0, \mathbf{p})$, i.e.,

$$\mathrm{Res}[f^{(4)}_{\lambda\sigma}(p_0, \mathbf{p}), p_0 = p^*_{0s}] = \frac{1}{6} \lim_{p_0 \to p^*_{0s}} \frac{d^3}{dp_0^3} \left[(p_0 - p^*_{0s})^4 \, \frac{p_\lambda p_\sigma}{(p_0 - p^*_{0s})^4 \, (p_0 + p^*_{0s})^4} \right] = \frac{1}{6} \lim_{p_0 \to p^*_0} \frac{d^3}{dp_0^3} \left[\frac{p_\lambda p_\sigma}{(p_0 + p^*_{0s})^4} \right]. \tag{A42}$$

Now, we take the required derivatives with care. To this end, we introduce the tensor $\alpha_{\lambda\sigma}(p_0, \mathbf{p}) = p_\lambda p_\sigma$, which admits at most two derivatives with respect to p_0. Thus, we obtain

$$\begin{aligned}\mathrm{Res}[f^{(4)}_{\lambda\sigma}(p_0, \mathbf{p}), p_0 = p^*_{0s}] &= \frac{1}{6} \lim_{p_0 \to p^*_{0s}} \frac{d^3}{dp_0^3} \left[\frac{\alpha_{\lambda\sigma}}{(p_0 + p^*_{0s})^4} \right] = \frac{1}{6} \lim_{p_0 \to p^*_{0s}} \frac{d^2}{dp_0^2} \left[\frac{\alpha'_{\lambda\sigma}}{(p_0 + p^*_{0s})^4} - 4 \frac{\alpha_{\lambda\sigma}}{(p_0 + p^*_{0s})^5} \right] \\ &= \frac{1}{6} \lim_{p_0 \to p^*_{0s}} \frac{d}{dp_0} \left[\frac{\alpha''_{\lambda\sigma}}{(p_0 + p^*_{0s})^4} - 8 \frac{\alpha'_{\lambda\sigma}}{(p_0 + p^*_{0s})^5} + 20 \frac{\alpha_{\lambda\sigma}}{(p_0 + p^*_{0s})^6} \right] \\ &= \frac{1}{6} \lim_{p_0 \to p^*_{0s}} \left[-12 \frac{\alpha''_{\lambda\sigma}}{(p_0 + p^*_{0s})^5} + 60 \frac{\alpha'_{\lambda\sigma}}{(p_0 + p^*_{0s})^6} - 120 \frac{\alpha_{\lambda\sigma}}{(p_0 + p^*_{0s})^7} \right],\end{aligned} \tag{A43}$$

where the prime denotes a derivative with respect to p_0. In order to evaluate the derivatives of the tensor $\alpha_{\lambda\sigma}(p_0, \mathbf{p})$, we separate it into its components as follows:

$$\alpha_{\lambda\sigma}(p_0, \mathbf{p}) = p_0^2 \delta^0_\lambda \delta^0_\sigma + p_0 p_i (\delta^0_\lambda \delta^i_\sigma + \delta^i_\lambda \delta^0_\sigma) + p_i p_j \delta^i_\lambda \delta^j_\sigma, \tag{A44}$$

such that $\alpha'_{\lambda\sigma} = 2p_0 \delta^0_\lambda \delta^0_\sigma + p_i (\delta^0_\lambda \delta^i_\sigma + \delta^i_\lambda \delta^0_\sigma)$ and $\alpha''_{\lambda\sigma} = 2\delta^0_\lambda \delta^0_\sigma$. Finally, we substitute these expressions results and take the limit $p_0 \to p^*_{0s}$. After further simplifications, we obtain

$$\mathrm{Res}[f^{(4)}_{\lambda\sigma}(p_0, \mathbf{p}), p_0 = p^*_{0s}] = \frac{s \delta^0_\lambda \delta^0_\sigma}{32(|\mathbf{p}|^2 + m^2)^{5/2}} - \frac{5 s p_i p_j \delta^i_\lambda \delta^j_\sigma}{32(|\mathbf{p}|^2 + m^2)^{7/2}} \tag{A45}$$

which is the result presented in the main text.

Appendix E. Evaluation of the Function $J_n(\mu, m)$

In Section 4.4, we introduced the function $J_n(\mu, m)$, defined by Equation (84). In this section, we present its detailed evaluation. We first perform the summation of the poles, i.e.,

$$J_n(\mu, m) = \int_{|m|}^{\infty} \frac{dp^*_0}{p^{*n}_0} \, [H(\mu - p^*_0) - H(\mu + p^*_0)]. \tag{A46}$$

The evaluation of the integral is simple, but not straightforward. The subtlety is based on the fact that there are two scales mass, $|m|$ and μ, and the result of the integral depends on how these compare. Let us consider the different cases separately.

We first consider the case of the chemical potential lying in the bandgap, i.e., $\mu < |m|$. In this case, the first Heaviside function vanishes, while the second Heaviside function is trivially fulfilled. This gives

$$J_n(\mu, m) = -\int_{|m|}^{\infty} \frac{dp_0^*}{p_0^{*n}} H(|m| - \mu) = -\frac{1}{(n-1)|m|^{n-1}} H(|m| - \mu). \tag{A47}$$

Substituting this result into Equation (83), we obtain the VPT in the bandgap ($\mu < |m|$), which corresponds to Equation (85) of the main text.

We now consider the case $\mu > |m|$, which means that the Fermi level lies within the finite density of electron states. In this case, the first Heaviside function establishes an upper limit on the integral, while the second Heaviside function is trivially fulfilled. Therefore, we obtain

$$J_n(\mu, m) = \left[\int_{|m|}^{\mu} \frac{dp_0^*}{p_0^{*n}} - \int_{|m|}^{\infty} \frac{dp_0^*}{p_0^{*n}}\right] H(\mu - |m|) = -\frac{1}{(n-1)\mu^{n-1}} H(\mu - |m|). \tag{A48}$$

The case $\mu < -|m|$, which corresponds to a Fermi level lying within the finite density of hole states, can be computed in a similar manner. We find

$$J_n(\mu, m) = -\int_{-\mu}^{\infty} \frac{dp_0^*}{p_0^{*n}} H(-\mu - |m|) = -\frac{1}{(n-1)(-\mu)^{n-1}} H(-\mu - |m|). \tag{A49}$$

Using these results, one can evaluate the VPT for a finite density of states. Substituting Equation (A48) into Equation (83), we obtain, for $\mu > |m|$,

$$\tilde{\Pi}^{\mu\nu}_{\text{odd}}(k, \mu) = -i\frac{1}{2h}\frac{m}{\mu}\epsilon^{\mu\beta\nu}k_\beta\left[1 + \frac{k^2}{12\mu^2} + \frac{|\mathbf{k}|^2}{4\mu^2}\left(1 - \frac{m^2}{\mu^2}\right)\right] H(\mu - |m|), \tag{A50}$$

while Equation (A49) yields, for $\mu < -|m|$,

$$\tilde{\Pi}^{\mu\nu}_{\text{odd}}(k, \mu) = +i\frac{1}{2h}\frac{m}{\mu}\epsilon^{\mu\beta\nu}k_\beta\left[1 + \frac{k^2}{12\mu^2} + \frac{|\mathbf{k}|^2}{4\mu^2}\left(1 - \frac{m^2}{\mu^2}\right)\right] H(-\mu - |m|). \tag{A51}$$

These equations are summarized in Equation (86) of the main text.

Appendix F. The Vector Potential

The integral we shall evaluate is defined by Equation (120), i.e.,

$$I(\mathbf{r}) = \int G_\mu(\mathbf{r}, \mathbf{r}')\, \delta(z')\, \phi(\mathbf{r}')\, d^3\mathbf{r}' = \int G_\mu(\mathbf{r}, \mathbf{r}'_\perp)\, \phi(\mathbf{r}'_\perp)\, d^2\mathbf{r}'_\perp. \tag{A52}$$

Using Green's function (117) and scalar potential (118), we obtain [44]

$$I(\mathbf{r}) = \frac{q}{4\pi^2(\epsilon_1 + \epsilon_2)(1/\mu_1 + 1/\mu_2)} \int \frac{1}{\sqrt{|\mathbf{r} - \mathbf{r}'_\perp|^2 + z^2}} \frac{1}{\sqrt{r'^2_\perp + z_0^2}}\, d^2\mathbf{r}'_\perp. \tag{A53}$$

Now, to evaluate this integral, we use the following integral representation:

$$\frac{1}{|\mathbf{r} - \mathbf{r}'|} = 4\pi \int \frac{d^2\mathbf{k}_\perp}{(2\pi)^2} e^{i\mathbf{k}_\perp \cdot (\mathbf{r}_\perp - \mathbf{r}'_\perp)} \frac{e^{-k_\perp|z-z'|}}{2k_\perp} \tag{A54}$$

Using this representation twice in Equation (A53), we obtain

$$I(\mathbf{r}) = \frac{q}{(\epsilon_1+\epsilon_2)(1/\mu_1+1/\mu_2)} \int d^2\mathbf{r}'_\perp \int \frac{d^2\mathbf{k}_\perp}{(2\pi)^2} e^{i\mathbf{k}_\perp\cdot(\mathbf{r}_\perp-\mathbf{r}'_\perp)} \frac{e^{-k_\perp|z|}}{k_\perp} \int \frac{d^2\mathbf{k}'_\perp}{(2\pi)^2} e^{i\mathbf{k}'_\perp\cdot\mathbf{r}'_\perp} \frac{e^{-k'_\perp z_0}}{k'_\perp}. \tag{A55}$$

Integration with respect to the coordinates $\mathbf{r}'_\perp$ produces the Dirac delta $(2\pi)^2\delta(\mathbf{k}_\perp - \mathbf{k}'_\perp)$, thus obtaining

$$I(\mathbf{r}) = \frac{q}{(\epsilon_1+\epsilon_2)(1/\mu_1+1/\mu_2)} \int \frac{d^2\mathbf{k}_\perp}{(2\pi)^2} e^{i\mathbf{k}_\perp\cdot\mathbf{r}_\perp} \frac{e^{-k_\perp(|z|+z_0)}}{k_\perp^2}, \tag{A56}$$

where we have carried out the $\mathbf{k}'_\perp$ integration. To evaluate this integral, we introduce polar coordinates, i.e., $d^2\mathbf{k}_\perp = k_\perp dk_\perp d\phi$, and choose the k_x axis along the vector $\mathbf{r}_\perp$. Therefore, in using that $\mathbf{k}_\perp\cdot\mathbf{r}_\perp = k_\perp r_\perp \cos\phi$ and performing the angular integration, we obtain

$$I(\mathbf{r}) = \frac{q}{2\pi(\epsilon_1+\epsilon_2)(1/\mu_1+1/\mu_2)} \int_0^\infty dk_\perp\, J_0(k_\perp r_\perp)\, \frac{e^{-k_\perp(|z|+z_0)}}{k_\perp}. \tag{A57}$$

With the help of this, one can evaluate the vector potential (120) as follows:

$$\mathbf{A}^{(0)}(\mathbf{r}) = -\alpha\,\hat{\mathbf{n}}\times\nabla I(\mathbf{r}) = \frac{q\alpha}{2\pi(\epsilon_1+\epsilon_2)(1/\mu_1+1/\mu_2)} \frac{x\hat{\mathbf{e}}_y - y\hat{\mathbf{e}}_x}{r_\perp} \int_0^\infty dk_\perp\, J_1(k_\perp r_\perp)\, e^{-k_\perp(|z|+z_0)}. \tag{A58}$$

The resulting integral is well known. The final result corresponds to Equation (121) of the main text.

References

1. Mechelen, V.; Jacob, Z. Quantum gyroelectric effect: Photon spin-1 quantization in continuum topological bosonic phases. *Phys. Rev. A* **2018**, *98*, 023842. [CrossRef]
2. Mechelen, V.; Jacob, Z. Viscous Maxwell-Chern-Simons theory for topological electromagnetic phases of matter. *Phys. Rev. B* **2020**, *102*, 155425. [CrossRef]
3. Mechelen, T.V.; Jacob, Z. Nonlocal topological electromagnetic phases of matter. *Phys. Rev. B* **2019**, *99*, 205146. [CrossRef]
4. Mechelen, T.V.; Jacob, Z. Photonic dirac monopoles and skyrmions: Spin-1 quantization. *Opt. Mater. Express* **2019**, *9*, 95. [CrossRef]
5. Avron, J.E.; Seiler, R.; Zograf, P.G. Viscosity of quantum Hall fluids. *Phys. Rev. Lett.* **1995**, *75*, 697. [CrossRef]
6. Avron, J.E. Odd viscosity. *J. Stat. Phys.* **1997**, *92*, 543. [CrossRef]
7. Hoyos, C.; Son, D.T. Hall Viscosity and Electromagnetic Response. *Phys. Rev. Lett.* **2012**, *108*, 066805. [CrossRef]
8. Hoyos, C. Hall viscosity, topological states and effective theories. *Int. J. Mod. Phys. B* **2014**, *28*, 1430007. [CrossRef]
9. Wen, X.G.; Zee, A. Shift and spin vector: New topological quantum numbers for the Hall fluids. *Phys. Rev. Lett.* **1992**, *69*, 953. [CrossRef]
10. Barredo-Alamilla, E.; Bobylev, D.A.; Gorlach, M.A. Axion electrodynamics without Witten effect in metamaterials. *Phys. Rev. B* **2024**, *109*, 195136. [CrossRef]
11. Gómez, A.; von Dossow, R.M.; Martín-Ruiz, A.; Urrutia, L.F. Lorentz invariance violation and the CPT-odd electromagnetic response of a tilted anisotropic Weyl semimetal. *Phys. Rev. D* **2024**, *109*, 065005. [CrossRef]
12. Gómez, A.; Martín-Ruiz, A.; Urrutia, L.F. Effective electromagnetic actions for Lorentz violating theories exhibiting the axial anomaly. *Phys. Lett. B* **2022**, *829*, 137043. [CrossRef]
13. Gómez, A.; Urrutia, L. The Axial Anomaly in Lorentz Violating Theories: Towards the Electromagnetic Response of Weakly Tilted Weyl Semimetals. *Symmetry* **2021**, *13*, 1181. [CrossRef]
14. Kapusta, J.I.; Gale, C. *Finite-Temperature Field Theory: Principles and Applications*; Cambridge Monographs on Mathematical Physics; Cambridge University Press: Cambridge, UK, 2011.
15. Bellac, M.L. *Thermal Field Theory*; Cambridge Monographs on Mathematical Physics; Cambridge University Press: Cambridge, UK, 1996.
16. Ikebe, Y.; Morimoto, T.; Masutomi, R.; Okamoto, T.; Aoki, H.; Shimano, R. Optical hall effect in the integer quantum hall regime. *Phys. Rev. Lett.* **2010**, *104*, 256802. [CrossRef]
17. Rosa, F.S.S.; Dalvit, D.A.R.; Milonni, P.W. Casimir interactions for anisotropic magnetodielectric metamaterials. *Phys. Rev. A* **2008**, *78*, 032117. [CrossRef]

18. Martín-Ruiz, A.; Escobar, C.A. Casimir effect between ponderable media as modeled by the standard model extension. *Phys. Rev. D* **2016**, *94*, 076010. [CrossRef]
19. Dziom, V.; Shuvaev, A.; Pimenov, A.; Astakhov, G.V.; Ames, C.; Bendias, K.; Böttcher, J.; Tkachov, G.; Hankiewicz, E.M.; Brüne, C.; et al. Observation of the universal magnetoelectric effect in a 3D topological insulator. *Nat. Commun.* **2017**, *8*, 15197. [CrossRef]
20. Brüne, C.; Liu, C.X.; Novik, E.G.; Hankiewicz, E.M.; Buhmann, H.; Chen, Y.L.; Qi, X.L.; Shen, Z.X.; Zhang, S.C.; Molenkamp, L.W. Quantum hall effect from the topological surface states of strained bulk HgTe. *Phys. Rev. Lett.* **2011**, *106*, 126803. [CrossRef]
21. Qi, X.-L.; Li, R.; Zang, J.; Zhang, S.-C. Inducing a magnetic monopole with topological surface states. *Science* **2009**, *323*, 1184. [CrossRef]
22. Martín-Ruiz, A.; Cambiaso, M.; Urrutia, L.F. Green's function approach to Chern-Simons extended electrodynamics: An effective theory describing topological insulators. *Phys. Rev. D* **2015**, *92*, 125015. [CrossRef]
23. Zang, J.; Nagaosa, N. Monopole current and unconventional hall response on a topological insulator. *Phys. Rev. B* **2010**, *81*, 245125. [CrossRef]
24. Sun, Q.; Dvorquez, E.; Pinto, F.A.; Mathpal, M.C.; Maze, J.R.; Gibson, B.C.; Greentree, A.D. Magnetic response of topological insulator layer with metamaterial substrate induced by an electric point source. *New J. Phys.* **2025**, *27*, 033021. [CrossRef]
25. Pinto, F.A.; Heitzer, R.C.; Dvorquez, E.; Rodriguez, R.; Sun, Q.; Greentree, A.D.; Gibson, B.C.; Maze, J.R. Magnetic field characterization of edge currents in quantum spin hall insulators. *New J. Phys.* **2025**, *27*, 013008. [CrossRef]
26. Novikov, V.A.; Shifman, M.A.; Vainshtein, A.I.; Zakharov, V.I. Calculations in external fields in quantum chromodynamics. *Tech. Rev. Fortsch. Phys.* **1984**, *32*, 585. [CrossRef]
27. Zuk, J.A. A Functional Approach to Derivative Expansion of the Effective Lagrangian. *Phys. Rev. D* **1985**, *32*, 2653. [CrossRef]
28. Fraser, C.M. Calculation of Higher Derivative Terms in the One Loop Effective Lagrangian. *Z. Phys. C* **1985**, *28*, 101. [CrossRef]
29. Aitchison, I.J.R.; Fraser, C.M. Derivative Expansions of Fermion Determinants: Anomaly Induced Vertices, Goldstone-Wilczek Currents and Skyrme Terms. *Phys. Rev. D* **1985**, *31*, 2605. [CrossRef]
30. Das, A.K.; Karev, A. The Derivative Expansion and the Anomaly at Finite Temperature. *Phys. Rev. D* **1987**, *36*, 623. [CrossRef]
31. Babu, K.S.; Das, A.K.; Panigrahi, P. Derivative Expansion and the Induced Chern-simons Term at Finite Temperature in (2 + 1)-dimensions. *Phys. Rev. D* **1987**, *36*, 3725. [CrossRef]
32. Anacleto, M.A.; Brito, F.A.; Holanda, O.B.; Passos, E.; Petrov, A.Y. Induction of the higher-derivative Chern-Simons extension in QED_3. *Int. J. Mod. Phys. A* **2016**, *31*, 1650140. [CrossRef]
33. Nascimento, J.R.; Passos, E.; Petrov, A.Y.; Brito, F.A. Lorentz-CPT violation, radiative corrections and finite temperature. *J. High Energy Phys.* **2007**, *2007*, 016. [CrossRef]
34. Leite, J.; Mariz, T. Induced Lorentz-violating terms at finite temperature. *Europhys. Lett.* **2012**, *99*, 21003. [CrossRef]
35. Leite, J.; Mariz, T.; Serafim, W. The induced higher derivative Lorentz-violating Chern–Simons term at finite temperature. *J. Phys. G* **2013**, *40*, 075003. [CrossRef]
36. Mariz, T.; Martinez, R.; Nascimento, J.R.; Petrov, A.Y. On perturbative aspects of a nonminimal Lorentz-violating QED with CPT-odd dimension-5 terms. *Eur. Phys. J. C* **2021**, *81*, 974. [CrossRef]
37. Kostelecky, V.A.; Mewes, M. Electrodynamics with Lorentz-violating operators of arbitrary dimension. *Phys. Rev. D* **2009**, *80*, 015020. [CrossRef]
38. Mewes, M. Higher-order Lorentz violation. In Proceedings of the 6th Meeting on CPT and Lorentz Symmetry, Bloomington, IN, USA, 17–21 June 2013; pp. 65–68
39. VKostelecky, A.; Lehnert, R.; McGinnis, N.; Schreck, M.; Seradjeh, B. Lorentz violation in Dirac and Weyl semimetals. *Phys. Rev. Res.* **2022**, *4*, 023106. [CrossRef]
40. Lisboa-Santos, L.; Reis, J.A.; Schreck, M.; Ferreira, M.M., Jr. Planar electrodynamics modified by higher-derivative terms. *Phys. Rev. D* **2023**, *108*, 115032. [CrossRef]
41. Peskin, M.E.; Schroeder, D.V. *An Introduction to Quantum Field Theory*; Addison-Wesley: Reading, PA, USA, 1995.
42. Srednicki, M. *Quantum Field Theory*; Cambridge University Press: Cambridge, UK, 2007.
43. Colladay, D.; Kostelecky, V.A. CPT violation and the standard model. *Phys. Rev. D* **1997**, *55*, 6760. [CrossRef]
44. Ibarra-Meneses, M.; Martín-Ruiz, A. Radiation of a short linear antenna above a topologically insulating half-space. *Eur. Phys. J. Plus* **2024**, *139*, 144. [CrossRef]

Disclaimer/Publisher's Note: The statements, opinions and data contained in all publications are solely those of the individual author(s) and contributor(s) and not of MDPI and/or the editor(s). MDPI and/or the editor(s) disclaim responsibility for any injury to people or property resulting from any ideas, methods, instructions or products referred to in the content.